# A Computer Model for Analyzing Multiconductor Signal Propagation in Distribution Line Carrier Networks

Montague E. Hardy, III

Center for Commuinications and Signal Processing
Department of Electrical and Computer Engineering
North Carolina State University

TR-89/27
December 1989

# ABSTRACT

Hardy, Montague E. A Computer Model for Analyzing Multiconductor Signal Propagation in Distribution Line Carrier Networks (under the direction of Sasan Ardalan)

A computer model for predicting multiconductor signal propagation in distribution line carrier networks is implemented into a computer program. A doubly-linked list is used to manage the information needed to store the network information such as source voltage and impedance, load impedance, length of a segment and number of phases. The algorithm for entering and analyzing a network along with plotting the magnitude of the voltage and current along the line is discussed and references are made to the program listings in the appendix.

Several test cases are simulated and the results are compared with the experimental results found earlier [6]. For the most part theoretical predictions matched up well with the experimental results although there were a few unexplained anomalies. The impedance and admittance per-unit length matrices were calculated using a technique described by Paul [9]. It is concluded that a closed form multiconductor signal propagation model and an accurate method for finding the impedance and admittance per-unit length matrices have been found and implemented in a computer program and this program accurately predicts signal trends in most cases.

# ACKNOWLEDGEMENTS

The author wishes to thank Dr. J.B. O'Neal, Jr. and Dr. Sasan Ardalan of North Carolina State University; Lou Gale, Dan Borowski and other members of Carolina Power and Light's Distribution Automation Unit; Ken Shuey of Westinghouse Electric Corporation, my family, friends and most importantly the Lord Jesus Christ for their invaluable guidance, encouragement and assistance in this research.

# TABLE OF CONTENTS

# LIST OF SYMBOLS

$\mathbf{L}$ - per-unit length inductance matrix

$\mathbf{C}$ - per-unit length capacitance matrix

$\mathbf{Z}$ - per-unit length impedance matrix

$\mathbf{Y}$ - per-unit length admittance matrix

$\gamma$ - propagation constant matrix

$\Gamma_L$ - reflection coefficient matrix at the load

$\Gamma_o$ - reflection coefficient matrix at the source

$\mathbf{Z_o}$ - characteristic impedance matrix

$\mathbf{Y_o}$ - characteristic admittance matrix

$\mathbf{Z_L}$ - load impedance matrix

$\mathbf{Y_L}$ - load admittance matrix

$\mathbf{Z_s}$ - source impedance matrix

$\mathbf{Y_s}$ - source admittance matrix

$\mathbf{V_s}$ - source voltage vector

$\mathbf{U}$ - identity matrix

$L$ - length of line or segment

$x$ - distance along the line (0 - L)

$\mathbf{Z_{in}}(0)$ - load impedance matrix seen at the source

$\mathbf{Y_{in}}(0)$ - load admittance matrix seen at the source

$\mathbf{V}(x)$ - voltage vector at a distance x

$\mathbf{I}(x)$ - current vector at a distance x

$R_{se}$ - resistance due to the skin effect

$a$ - constant used in the calculation of $R_{se}$

$R_o$ - dc resistance of the conductor

$\lambda$ - transmission line wavelength

$vf$ - velocity factor

$\varepsilon_r$ - relative dielectric constant of the conductor (assumed to be unity)

$h_i$ - the heigth of conductor i above the ground

$hr_i$ - an arbitrary reference distance to conductor i

$d_{ij}$ - the center-to-center separation from conductor i to conductor j

$d_{ij}^*$ - the center-to-center separation between conductor i and the image of conductor j

$n_s$ - number of outer strands

$n_c$ - number of inner (core) strands

$r_i$ - outer radius of conductor i

$r_s$ - radius of the outer strands

$r_c$ - radius of the inner (core) strands

r - effective outer conductor radius

q - effective inner (core) radius

t - effective thickness of the hollow conductor

$A_s$ - total cross-sectional area of the outer strands

$A_{cond}$ - total cross-sectional area of metal in the hollow conductor

f - frequency ( 25 kHz for all test cases)

$\rho$ - resistivity of the conductor (for aluminum: $2.62 \times 10^{-8}$ $\Omega$-m, steel: $70 \times 10^{-8}$ $\Omega$-m)

c - speed of light in air = $3 \times 10^8$ m/sec = $186.42 \times 10^3$ miles/sec

$\mu_o$ - permeability of free space = $4\pi \times 10^{-7}$ H/m

$\varepsilon_o$ - permittivity of free space = $8.854 \times 10^{-12}$ F/m

# Chapter 1

## Introduction

A great deal of research has been done in distribution line carrier (DLC) technology in the past decade by the Electric Power Research Institute (EPRI) and others. DLC communications employ the power distribution systems as media for the transmission of information. These systems enable utilities to implement distribution automation applications such as load control, remote meter reading, capacitor bank dispatch and outage location. DLC uses two-way communications from a central point to many remote locations in a radial tree-topology network. It is difficult to achieve uniform signal strengths in such a complex network consisting of multiple branches and constantly varying user loads. Also, standing wave patterns present a problem that can not easily be predicted in a complex network [1,2].

A series of DLC studies have been conducted in a controlled network environment. Such studies were based on experimental measurements performed at Carolina Power and Light's distribution test facility [3]. Hemminger [4, pg 48] found that a termination resistance of 450 Ω was most effective in eliminating a standing wave pattern on a completely unloaded single phase line and that the losses were considerably less than 1 dB/mile. He found that the velocity of propagation on an unloaded overhead line was approximately 95% the speed of light in air [pg 46]. He also found that distribution transformers present over 10 kΩ magnitude impedance and that adding six transformers per mile reduced the velocity

of propagation to 85% of the speed of light in air. Borowski [5] later extended the single-phase network to include branching and analyzed network response to line parameter variations. Suh [6] performed several signal propagation measurements on multiconductor networks at the test facility. Various line and load configurations were considered to show the effect of coupling between the phases and standing wave patterns. Suh also found that a uniform three-phase system consisting of homogeneous conductors of equal length can be considered as a single-phase "bundled conductor" when the same boundary conditions are imposed on each of the phases. Riddle, Ardalan and Suh [7] derived a set of equations modeling multiple conductor systems (shown in chapter 2). Riddle [8] implemented these equations into a computer program and compared his computer results to the uniform conductor length experimental results found by Suh. These equations were used instead of ABCD parameters, as that used by General Electric [1,2], mainly because the voltage and current can be found at any point along the line which is very useful in the analysis and understanding of the standing wave effects.

In chapter 2, the multiconductor transmission line equations are listed and described briefly. Chapter 3 describes the derivation of the per-unit length impedance and admittance matrices from Paul [9]. Chapter 4 describes the network analysis computer program "3-2-1" written by the author. Source listings are referred to and listed in the appendix. Chapter 5 presents a comparison of computer test runs from "3-2-1" to the experimental results from Suh. Chapter 6 shows various computer test runs from "3-2-1" where a load termination with the value as the

characteristic impedance is placed at various points along the line and at the source. Finally, chapter 7 shows the importance of calculating accurate per-unit length impedance and admittance matrices and also discusses the future of transmission line modeling, and lists the conclusions.

# Chapter 2

## The Multiconductor Transmission Line Equations

In [7], a set of new and compact equations were derived for solving a system of multiconductor transmission lines with an arbitrary source and load termination. These equations are very suitable for implementation on a computer. The advantage of using these equations over the generally used ABCD parameters is that the voltage and current can be found at any point along the line not just at the beginning and end of the line.

Figure 2.1 shows a general schematic diagram of a multiconductor network. $\mathbf{V_S}$ is the nx1 source voltage vector, $\mathbf{Y_S}$ and $\mathbf{Y_L}$ are the nxn source and load admittance matrices, respectively with n being the number of phases in the network. L is the length of the line and x is a distance anywhere along the line. $\mathbf{V}(x)$ and $\mathbf{I}(x)$ are the voltage and current respectively at a distance x along the line.

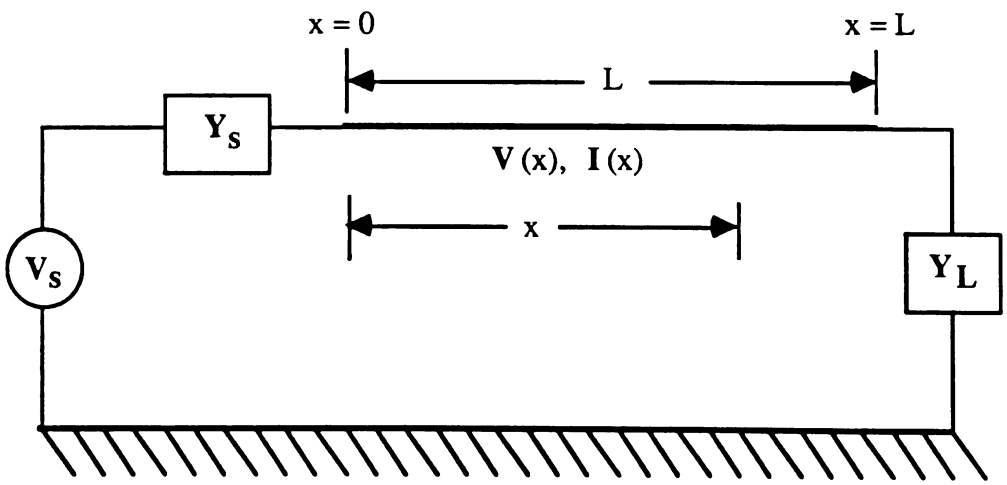


Figure 2.1 Schematic diagram of a typical transmission line

Figure 2.2 shows a schematic diagram of the same diagram in Figure 2.1 with the load admittance "rolled back" to the source. The load admittance seen at the source is denoted by the nxn matrix $\mathbf{Y_{in}}(0)$. $\mathbf{I}(0)$ is the source current injected into the network and $\mathbf{V}(0)$ is the voltage at the beginning of the transmission line after $\mathbf{Y_S}$. $\mathbf{I}(0)$ and $\mathbf{V}(0)$ are both nx1 vectors.

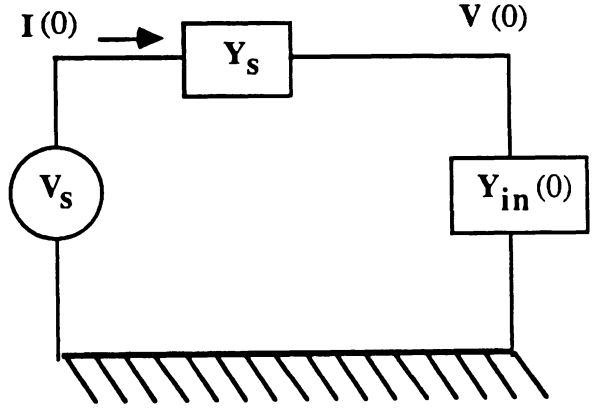


Figure 2.2 Schematic diagram of a typical transmission line with the load admittance "rolled back" to the source

As shown in [7], $\mathbf{Y_{in}}(0)$ is given by equation (2.1) below. $\mathbf{U}$ is the identity matrix, $\Gamma_o$ is the reflection coefficient matrix at the source and $\mathbf{Z_o}$ is the characteristic impedance matrix.

$$\mathbf{Y_{in}}(0) = \mathbf{Z_{in}}(0)^{-1} = \mathbf{Z_o}\ (\mathbf{U} + \Gamma_o)\ (\mathbf{U} - \Gamma_o)^{-1} \qquad (2.1)$$

Here $\Gamma_o$, $\Gamma_L$ and the propagation constant, $\gamma$, are given by equations (2.2a, b, and c) respectively. The characteristic admittance, $\mathbf{Y_o}$, is given by equation (2.2d).

$$\Gamma_o = e^{-\gamma L}\,\Gamma_L\,e^{-\gamma L} \tag{2.2a}$$

$$\Gamma_L = [Z_L\,Y_o + U]^{-1}[Z_L\,Y_o - U]$$

$$= [Z_L - Z_o][Z_L + Z_o]^{-1}$$

$$= [Y_o - Y_L][Y_o + Y_L]^{-1} \tag{2.2b}$$

$$\gamma = \sqrt{Z\ Y} \tag{2.2c}$$

$$Y_o = \sqrt{Y\ Z^{-1}} = Z_o^{-1} \tag{2.2d}$$

"Rolling" the admittances back to the source is the first step in the analysis of a transmission line network (Note: "Rolling" or "rolling back" can be thought of as finding the equivalent impedance of a single-phase load moved back a fraction of a wavelength on the Smith Chart.). Once the admittance has been "rolled back" to the source, the source current $I(0)$ and the voltage at the source $V(0)$ can be calculated by equations (2.3a and b). $V(0)$ and $I(0)$ are found by using voltage division and Ohm's Law respectively.

$$V(0) = Z_{in}(0)[Z_s + Z_{in}(0)]^{-1}\,V_s \tag{2.3a}$$

$$I(0) = Y_{in}(0)\,V(0) \tag{2.3b}$$

Once $\mathbf{V}(0)$ and $\mathbf{I}(0)$ are found then the the voltage and current at any distance x along the line can be found by equations (2.4a and b) below.

$$\mathbf{V}(x) = \left[\mathbf{U} + e^{\gamma(x-L)}\,\Gamma_{\mathbf{L}}\,e^{\gamma(x-L)}\right] e^{-\gamma x} \left[\mathbf{U} + e^{-\gamma L}\,\Gamma_{\mathbf{L}}\,e^{-\gamma L}\right]^{-1} \mathbf{V}(0) \tag{2.4a}$$

$$\mathbf{I}(x) = \mathbf{Y_0} \left[\mathbf{U} - e^{\gamma(x-L)}\,\Gamma_{\mathbf{L}}\,e^{\gamma(x-L)}\right] e^{-\gamma x} \left[\mathbf{U} - e^{-\gamma L}\,\Gamma_{\mathbf{L}}\,e^{-\gamma L}\right]^{-1} \mathbf{Z_0}\,\mathbf{I}(0) \tag{2.4b}$$

When implemented on a computer, voltage and current points can be calculated and stored in arrays; then magnitude plots of voltage and current versus distance can be generated.

# Chapter 3
# Derivation of the Per-Unit Length Impedance (Z) and Admittance (Y) Matrices

## 3.1. Derivation of the Per-Unit Length Inductance (L) and Capacitance (C) Matrices

In [9], a method was presented to compute the per-unit length inductance and capacitance matrices used in multiconductor transmission line models. Note that the permeability of all the conductors will be considered to be that of free space, $\mu_o$; and $\varepsilon_o$ will denote the free space permittivity. Figure 3.1 shows a system of n wires above a ground plane.

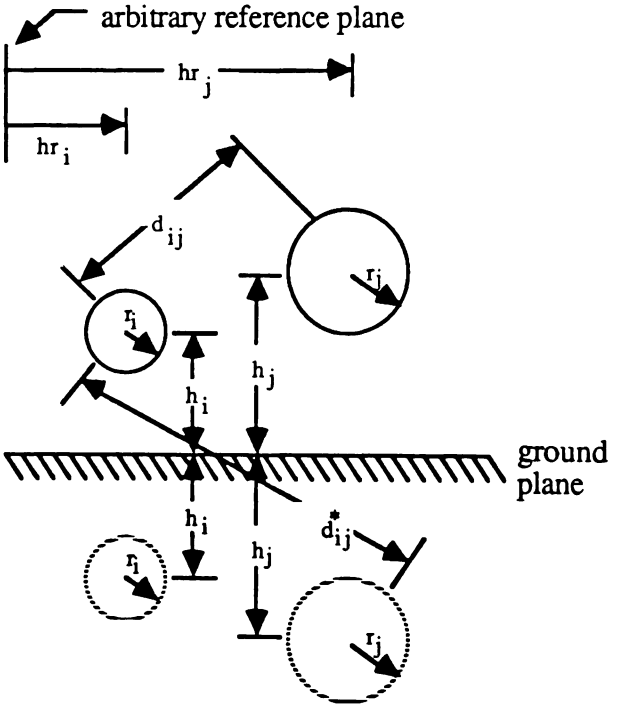


Figure 3.1. A system of n wires above a ground plane

In Figure 3.1, $d_{ij}$ is the center-to-center separation of the $i^{th}$ wire and the $j^{th}$ wire for i, j = 1,...,n. $d_{ij}^*$ is the center-to-center separation between the $i^{th}$ wire and the image of the $j^{th}$ wire. $d_{ij}$ and $d_{ij}^*$ are given by equations (3.1a and b) below.

$$d_{ij} = \sqrt{(hr_i - hr_j)^2 + (h_i - h_j)^2} \qquad (3.1a)$$

$$d_{ij}^* = \sqrt{(h_i + h_j)^2 + (hr_j - hr_i)^2} = \sqrt{d_{ij}^2 + 4h_ih_j} \qquad (3.1b)$$

Figure 3.2 shows the configuration of the overhead distribution lines at the CP&L test facility where all of the experimental measurements in [6] where made. Hemminger [4] found that approximately 70% of the primary current returns through the earth's surface except for a few poles at either end of the line. The exact percentage generally varies with the type of soil and its moisture content. One assumption made in the derivation of the **Z** and **Y** per-unit matrices is that all of the primary current returns through the earth's surface and as a result the neutral wire can be ignored (We later found that this may not be a good assumption; see the Conclusions in Chapter 7.). This eliminates the need for 4x4 matrices for the configuration shown in Figure 3.2. Suh [6] mathematically showed how the neutral wire can be eliminated from the matrix in the case of a four conductor system. Equations (3.2a and b) shows the calculation of the nxn inductance (**L**) matrix where n is the number of wires or phases in the network [7]. $\mathbf{C_o}$ is the nxn per-unit length transmission line capacitance matrix.

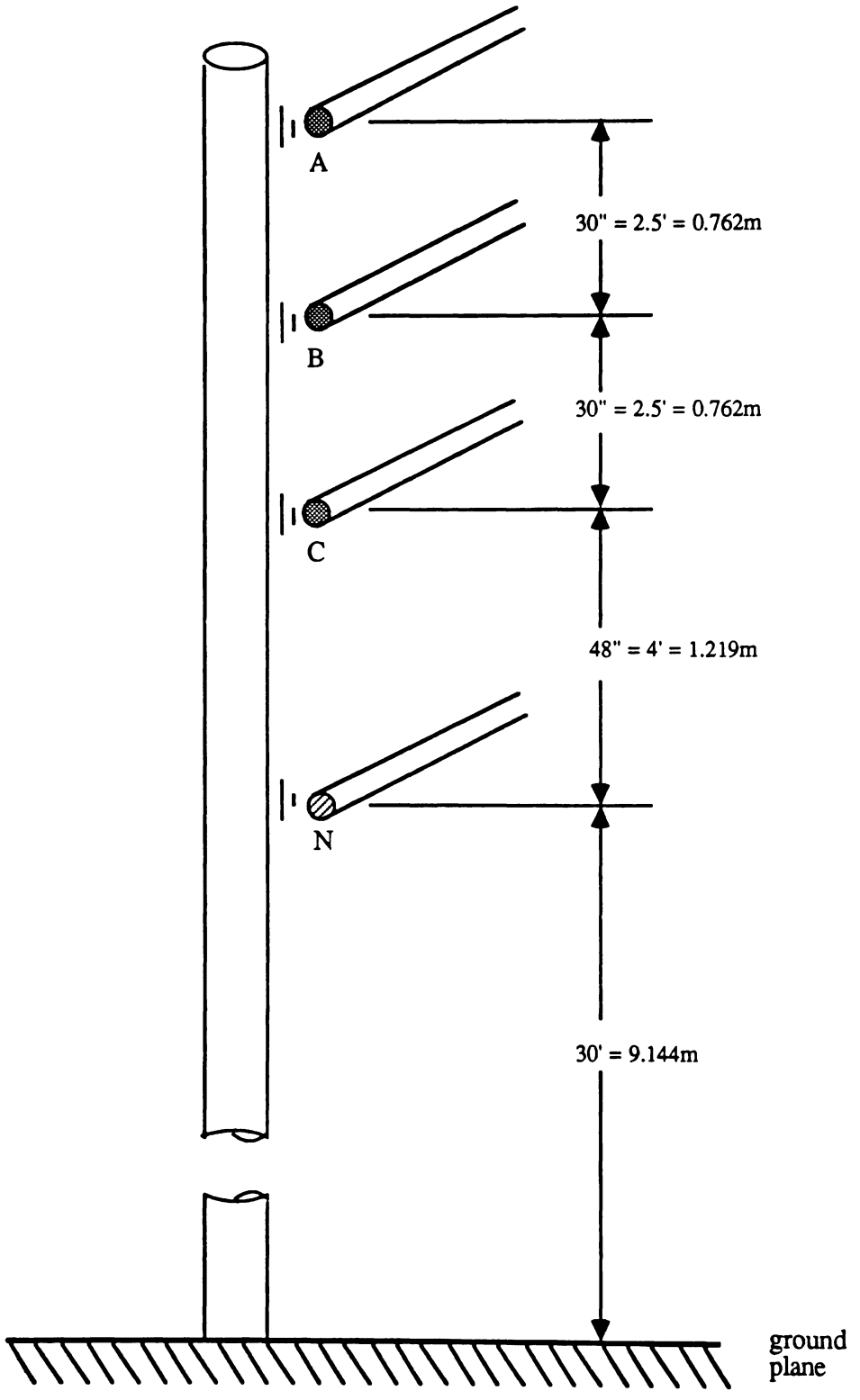


Figure 3.2 Conductor configuration for vertical geometry at test facility

$$L_{ii} = \mu_o \varepsilon_o C_{oii}^{-1} = \frac{\mu_o}{2\pi} \ln\left(\frac{2h_i}{r_i}\right) \qquad (3.2a)$$

$$L_{ij} = \mu_o \varepsilon_o C_{oij}^{-1} = \frac{\mu_o}{2\pi} \ln\left(\frac{d_{ij}^*}{d_{ij}}\right) \qquad (3.2b)$$

for i, j = 1,...,n.

Once the inductance matrix has been found, the nxn capacitance (C) matrix is calculated by equation (3.3) below where $\varepsilon_r$ is the relative dielectric constant of the conductor and is assumed to be unity.

$$C = \mu_o \varepsilon_o \varepsilon_r L^{-1} \qquad (3.3)$$

## 3.2. Calculation of the Skin Effect

Skin effect is the tendency alternating currents to flow with greater density near the outside of conductors [10]. It increases the resistance and to a lesser extent the reactance as the frequency, resistivity and area of cross section of the conductor increases. The type conductor used at the test facility for above ground is aluminum conductor steel reinforced (ACSR) #2. See Figure 3.3a for the stranding arrangement for the ACSR #2 conductor [11].

Since the steel core has a conductivity which is almost 27 times lower than that of the aluminum strands [12] and due to the skin effect, most of the current will be flowing in the aluminum strandings. The presence of the steel core gives the conductor much of the same effect as that of a

hollow tube [10,13]. See Figure 3.3b to see how the current density is assumed to be distributed in the hollow conductor model.

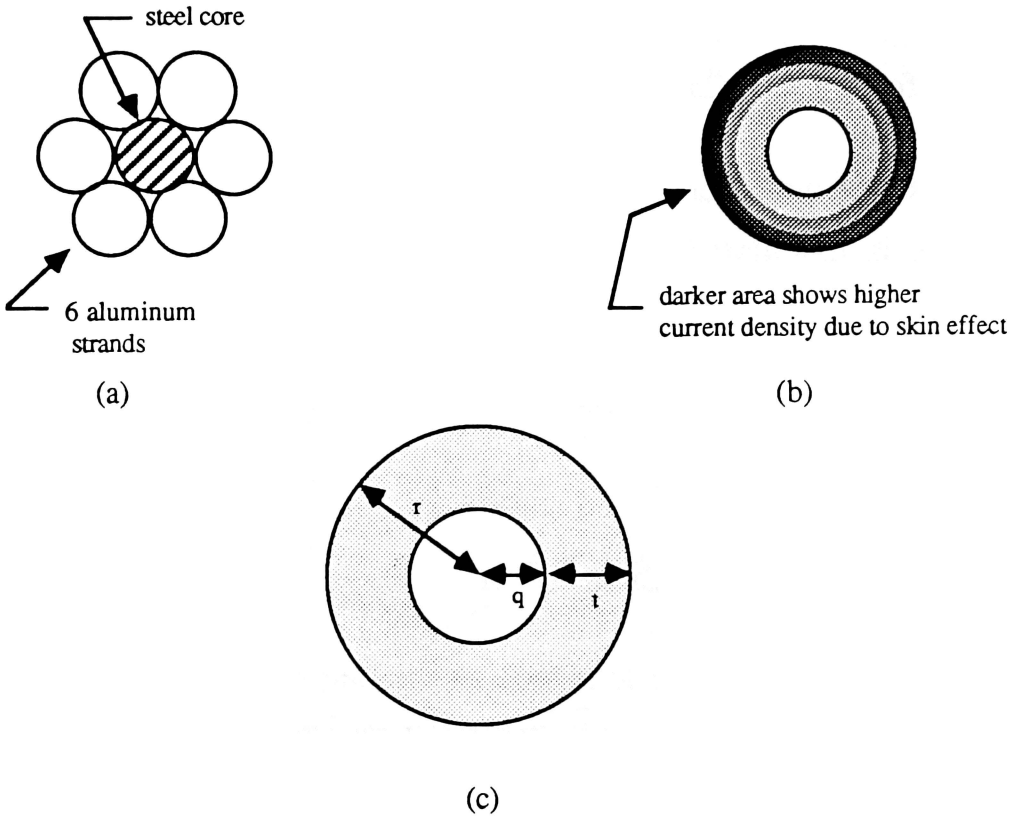


Figure 3.3. a) Stranding arrangement for a ACSR #2 conductor
b) hollow conductor showing the distribution of current density due to skin effect
c) hollow conductor showing conductor dimensions

In [14], Dwight derives the resistance ($R_{se}$) due to the skin effect for a hollow conductor. The inductance due to the skin effect is negligible since the flux inside the metal is extremely small compared with the flux

(c)

but the equation simplifies for high frequencies (see equations (3.4a-c)). Figure 3.3c shows the variables used to represent the hollow conductor.

$$R_{se} = \frac{R_o at(q + r)}{2r\sqrt{2}} \tag{3.4a}$$

where $$R_o = \frac{\rho}{\pi(r^2 - q^2)}\ \Omega \tag{3.4b}$$

$$a = \sqrt{\frac{2\pi f \mu_o}{\rho}}\ m^{-1} \tag{3.4c}$$

for aluminum [12]:

$\rho = 2.62 \times 10^{-8}\ \Omega$-m

The thickness, t, of the hollow conductor is found by finding the total cross-sectional area of the outer strands, $A_s$, and letting that be the area of the metal in the hollow conductor, $A_{cond}$ [10,15]. The derivation below shows how t and q are found.

$$A_s = n_s \pi r_s^2 \tag{3.5a}$$

$$A_{cond} = \pi(q + t)^2 - \pi q^2 \tag{3.5b}$$

Setting (3.5a) equal to (3.5b) and solving for t yields:

$$t^2 + 2qt - n_s r_s^2 = 0 \tag{3.5c}$$

The positive root of (3.5c) yields:

$$t = -q + \sqrt{q^2 + n_s r_s^2} \tag{3.5d}$$

Similarly, the radius of the core, q, is given by equation (3.6) below.

$$q = r_c\sqrt{n_c} \qquad (3.6)$$

for ACSR #2:

$n_s = 6$, $n_c = 1$, $r_s = r_c = 1.336$ millimeters = 0.0526 inches

## 3.3. The Final Step in Calculating the **Z** and **Y** Per-Unit Length Matrices

The **L** and **C** found by equations (3.2a and b) and (3.3) are multiplied by the angular frequency, $2\pi f$, and make up the imaginary part of the **Z** and **Y** per-unit length matrices respectively. The off-diagonal resistance and conductance terms of **Z** and **Y** are set to zero by assuming no corona or interphase losses. The diagonal conductance term of the **Y** matrix is set to a small number so that a problem in overflow will not occur when matrix inversion is performed. Realistically, this would represent the small losses over the insulators and poles due to contamination. The $R_{se}$ calculated in equation (3.4a) will be the resistive diagonal component of the **Z** matrix. Figure 3.4a and b shows the calculated **Z** and **Y** per-unit matrices for the ACSR #2 conductor at 25 kHz.

$$\mathbf{Z} = \begin{bmatrix} 3.16 + j439.20 & 0.00 + j172.44 & 0.00 + j135.35 \\ 0.00 + j172.44 & 3.16 + j435.86 & 0.00 + j168.30 \\ 0.00 + j135.35 & 0.00 + j168.30 & 3.16 + j432.23 \end{bmatrix} \quad \Omega/\text{mile}$$

(a)

$$\mathbf{Y} = \begin{bmatrix} 1.61e\text{-}09 + j1.98e\text{-}03 & 0.0 - j6.42e\text{-}04 & 0.0 - j3.72e\text{-}04 \\ 0.0 - j6.42e\text{-}04 & 1.61e\text{-}09 + j2.13e\text{-}03 & 0.0 - j6.27e\text{-}04 \\ 0.0 - j3.72e\text{-}04 & 0.0 - j6.27e\text{-}04 & 1.61e\text{-}09 + j2.00e\text{-}03 \end{bmatrix} \mho/\text{mile}$$

(b)

Figure 3.4 (a) Calculated impedance per-unit length matrix, (b) Calculated admittance per-unit length matrix

## 3.4 The Calculation of the Characteristic Impedance $\mathbf{Z_o}$

Once the **Z** and **Y** per-unit length matrices have been calculated then the characteristic impedance matrix, $\mathbf{Z_o}$, can be calculated by equation (3.5) below.

$$\mathbf{Z_o} = \sqrt{\mathbf{Z}\,\mathbf{Y}^{-1}} \qquad (3.5)$$

The resulting matrix is shown below.

$$\mathbf{Z_o} = \begin{bmatrix} 520.86 - j1.02 & 204.49 + j1.65 & 160.50 + j0.94 \\ 204.49 + j1.65 & 516.90 - j1.16 & 199.59 + j1.43 \\ 160.50 + j0.94 & 199.59 + j1.43 & 512.60 - j0.96 \end{bmatrix} \quad \Omega$$

# Chapter 4
# Description of the Network Analysis Computer Program "3-2-1"

## 4.1. General Description of "3-2-1"

Using the equations described in chapters 2 and 3, the computer program "3-2-1" has been written in C [16,17] to enable a user to enter the parameters of a distribution line network, analyze a network that can change from three phases to two phases to a single phase with loads anywhere along the line and obtain plots of the magnitude of the voltage and current along the individual phases. "3-2-1" uses a doubly-linked list [17] to store and manage the network entered. Dynamic allocation of memory is used for the complex and real matrices and arrays. Figure 4.1a shows a generalized three phase distribution line network with n nodes. Note that loads can be put between the phases but is not shown in Figure 4.1a. Node 1 must have three phases but nodes 2 to n can have 3, 2 or 1 phases as long as the number of phases are the same or decreasing (e.g. if node 3 has two phases then node 4 can have one or two phases but not three). Figure 4.1b shows a more generalized diagram of Figure 4.1a. Figure 4.1c shows the doubly-linked list representation of the distribution line network. A doubly-linked list allows the previous and next node information to be accessed. See the header file *ll_main.h* in appendix A for the structure declaration of the node and header in Figure 4.1c. By using node pointers [16,17], the header can easily access the information in the first and last node in the network and each node can access the node before it and after it. This is a necessary feature when "rolling" the load

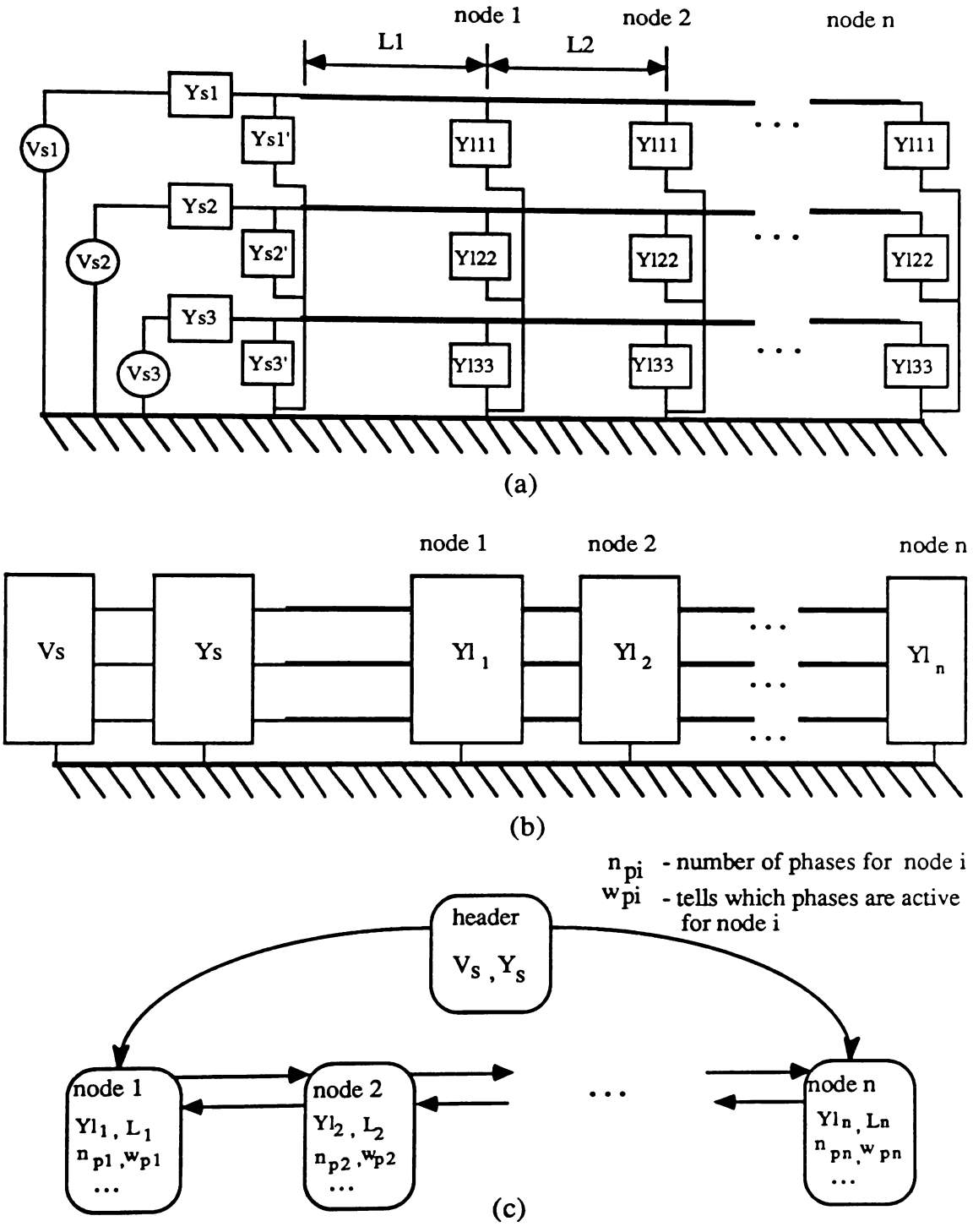


Figure 4.1 (a) Schematic diagram of a 3-phase distribution line network with n loads distributed along the line, (b) generalized network, (c) doubly-linked list representation of a distribution line network

admittances back to the source. (Note: See Chapter 2 for the meaning of "rolling" or "rolling back".) Many of the parameters, such as the eigensystem (eigenvalues and eigenvectors) for the propagation constant and the reflection coefficients (see *ll_main.h* in Appendix A), needed in the analysis are calculated when the admittances are "rolled back", therefore each node also stores this information. Once a network has been analyzed, the magnitude of the voltage and/or current can be displayed on the terminal and/or sent to a data file where it can then be plotted.

## 4.2. Using "3-2-1"

The user is allowed to change the source voltage and admittances. (Note: the notation for admittances is used instead of impedances since admittances add in parallel, which is convenient when the load admittance is "rolled back" to the source since the loads are distributed in parallel. Also, when open circuit loads are specified, zero admittance is more easily specified than high resistance.) When each node is entered, the user is prompted for the node name, load admittance, line length for that segment and the number and description of the phases that are active.

When the user runs "3-2-1", the main menu appears and has the options shown in Figure 4.2 below. When any of the options are selected and completed then the user is returned to the main menu.

```
A - Edit a node or the source
B - Insert a node
C - Delete a node
D - View a node
E - Print whole network info. to screen
F - Send network to a file
G - Read in network from a file
H - Print file to screen
I - Roll back load to the source
J - Analyze network
K - Output voltage and/or current
L - Delete the list
M - Terminate a node with Zo
X - Exit to system

Choice:
```

Figure 4.2 The main menu of the computer program "3-2-1"

The user can either read in a network data file or create a new one. If he reads in a data file then he can edit it and store it back in the same data file or a different one. If a new network is created then it can also be stored in a data file.

Once the network is read in, the load admittances are "rolled back" to the source (selection "I" in Figure 4.2). The user is first asked asked if he wants to change the conductor geometry (height of the conductors above

ground and the spacings between the conductors) or the ACSR conductor properties (number of inner and outer strands and the radius of the inner and outer strands) for the entire network. The menu shown in Figure 4.3 is displayed before the load admittances are "rolled back".

```
A - Absolute horizontal distance
B - Height of lines above ground

C - Number of outer strands (6)
D - Number of inner (core) strands (1)
E - Radius of outer strands (1.336e-03 m)
F - Radius of inner (core) strands (1.336e-03 m)
G - View configuration

X - Exit to roll load back to source

Choice:
```

Figure 4.3 Menu for changing conductor geometry and properties when "rolling" load admittances back to the source

Then the load admittances are "rolled back" to the source storing the load admittance seen at each node looking into the network along the way. This is done so that in the analysis, the admittance looking into each node is known. Many of the parameters needed in the analysis are also needed therefore calculated and stored in each node in the "rolling back" process.

The user can also choose to put the calculated characteristic impedance or any scalar factor of it as the load at any node including the

source impedance (selection "M" in Figure 4.2). The procedure is to first enter or read in the network you want to analyze, "roll" the load impedances back to source to calculate the characteristic impedance for each node, then specify the nodes you wish to put the characteristic impedance, "roll" the load impedances back to the source again since some or all of the loads have changed.

Then the analysis can be done where the voltage and current at points along the line can be calculated and stored in arrays for each node. Each segment is analyzed independently.

## 4.3. Description of the files used in "3-2-1"

The appendix contains the source listings of most of the files used by "3-2-1". Below is a short description of the purpose of each file. The files marked with an asterisks (*) are not listed in the appendix.

*standard.h* *: contains definitions for debugging and profiling purposes throughout the source files in "3-2-1"

*ll_main.h* : contains all of the structure declarations for the doubly-linked list, the **Z** and **Y** per-unit length matrices and the coupling system geometry

*cx.h* : contains declarations for the complex math routines

*ll_const.h* : contains definitions used in the calculation of the resistance and inductance due to the skin effect and the **Z** and **Y** per-unit length matrices

*ll_main.c* : contains high-level functions to edit, insert, view and delete nodes in the doubly-linked list; asks the user to enter node information about the network; contains the main program which displays and gets the user response from the Main Menu

*ll_lists.c* : contains low-level functions to manage the doubly-linked list

*ll_newzy.c* : calculates the **Z** and **Y** per-unit length matrices

*ll_calcgamyo.c* : calculates and stores the propagation coefficient matrix, characteristic admittance and impedance matrices and the eigensystem (eigenvalues and eigenvectors) for the propagation coefficient matrix for a single node

*ll_rollall.c* : controls the "rolling back" process of the load impedances to the source, calls *ll_lowroll.c* to "roll back" each segment

*ll_lowroll.c* : calculates the admittance seen looking into a single segment of distribution line, which includes the load at

the beginning of that segment, due to an end load admittance or a previously "rolled" back admittance

*ll_anlyzall.c* : controls the analysis process of the network, initializes matrices appropriately before calling *ll_lowanlyz.c*

*ll_lowanlyz.c* : calculates and stores the voltage and current points into dynamically allocated arrays for a single segment of line

*ll_plotset.c* *: sends the voltage and current points to the terminal to view and/or sends them to a data file where they can then be plotted

*cmat_eigens.c* *: computes the eigenvalues and eigenvectors of a nxn complex matrix

The files, cx_complex.c, mat_matrix.c and cmat_matrix.c, contains functions to perform operations on complex numbers, real matrices and complex matrices and vectors respectively. See Figure 4.4 for a general flow chart of how the files in "3-2-1" are used.

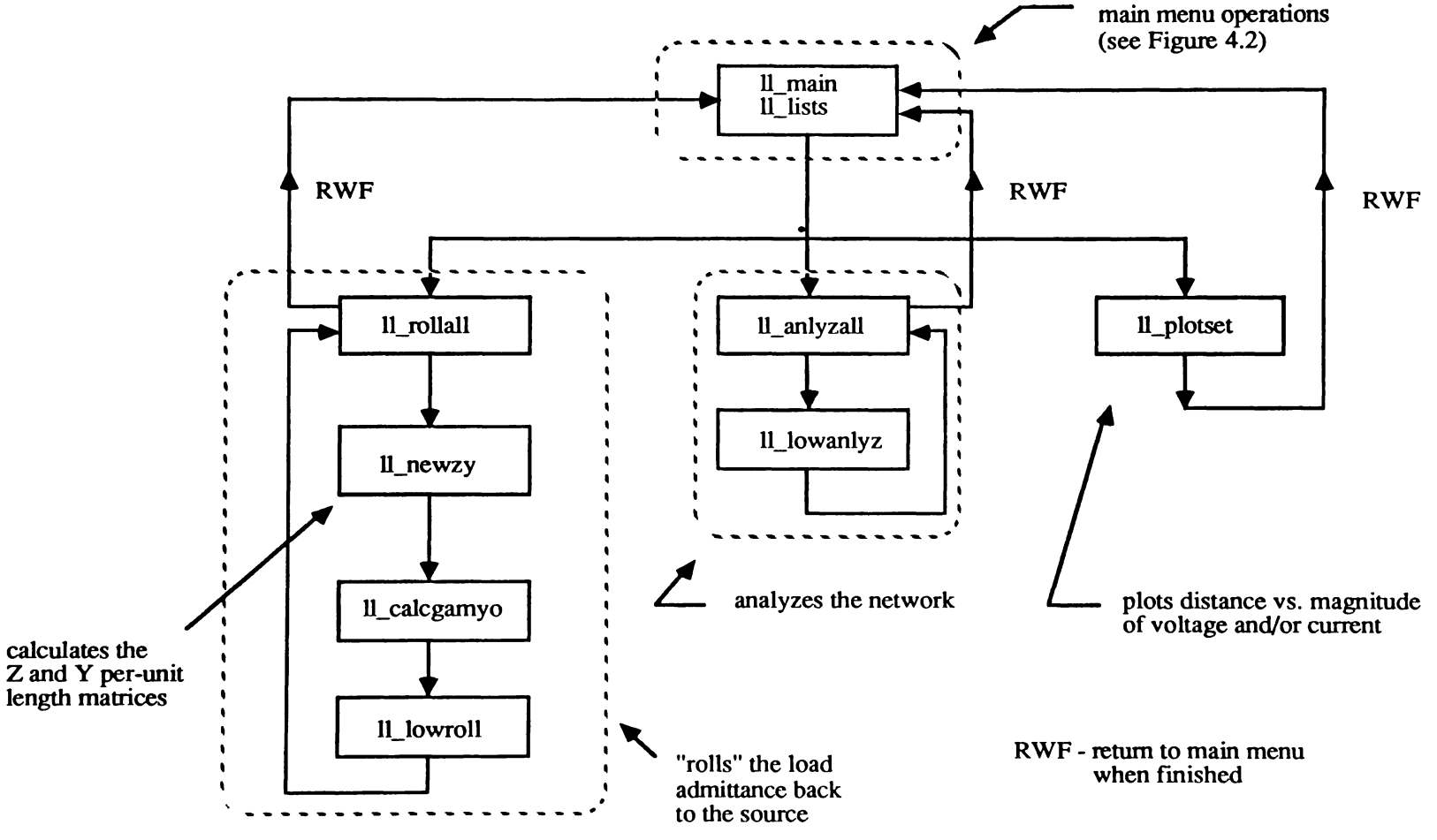


Note: the matrix operation files, cx_complex.c, mat_matrix.c, cmat_matrix.c, cmat_eigens.c and cmat_init.c, are used throughout the files shown above

Figure 4.4 A general flow chart of how the files in "3-2-1" are used

# Chapter 5

## A Comparison of the Calculated and Experimental Results

### 5.1. Introduction

Several sets of measurements were made on different configurations of the three-phase overhead distribution lines at Carolina Power and Light's Distribution Automation Test Facility by Suh [6]. In each test case, the injected signal was a 50 volt peak-to-peak sinusoid ($V_S$) with a frequency of 25 kHz. The source impedance was always 5 Ω when $V_S$ was applied to a phase. The 25 kHz frequency was chosen so that at least one node and antinode could be detected in the subsequent standing wave patterns. With a velocity of propagation of 95% the speed of light in air [4], this corresponds to a voltage minima at a quarter-wavelength of 1.77 miles or 9350 feet (see equation (5.1) below).

$$\lambda/4 = \frac{vf\,c}{4f} = \frac{0.95 * 186.42 \times 10^3 \text{ miles/sec}}{4 * 25 \times 10^3 \text{ /sec}} = 1.77 \text{ miles} \qquad (5.1)$$

Suh describes how the signal was generated and injected on the line and how the measurements were taken. For the test cases, measurements were taken every 0.4 mile. Figures 5.1-14, at the end of the chapter, show 14 different test cases; the scattered points are the experimental measurements and the lines are the calculations ran using the computer program "3-2-1".

## 5.2. Test Cases with Uniform Line Lengths

In the four configurations of test 1 (Figures 5.1-5.4) the length of the line was chosen to be a half-wavelength (approximately 3.59 miles). Figure 5.1a shows the schematic diagram for the line configuration of test 1a. An open-circuit load is used for this test case and phases B and C are not connected at the source and at the load. Figure 5.1b shows the magnitude of the voltage versus distance which displays the typical standing wave pattern for this half-wavelength line. Phases B and C have been omitted in the experimental plots in each test case where those phases were unconnected at the source and the load since the measurements were questionable. It is thought that when the test probes were connected to the floating phase, the voltage was shorted to ground. Current readings were obtainable for the floating phases since a current probe was used which clamps around the wire not on it. Figure 5.1c shows the corresponding magnitude of current in milliamps versus distance in miles for the experimental case. There is measurable coupling on phases B and C from phase A. The general shape of the corresponding calculation and experimental results match up well. The biggest difference is that the magnitude of the calculated current is not as high as the measured current. This is a problem that will be seen in most of the test cases. These comparative results show the importance of calculating accurate **Z** and **Y** per-unit length matrices. In any case where the calculation does not match up well with the experiment, either there was error in the measurements or inaccuracies in the calculated **Z** and **Y** per-unit length matrices.

Figure 5.2 shows the test case for 1b where all three phases are energized and all boundary conditions are identical for each phase. In this case, the three phase system can be considered to be a single-phase bundled conductor. See Figure 5.2b for the voltage plot for the bundled conductors. The currents in Figures 5.2c show that the phase currents are not exactly equal at all points. This can be attributed to such factors as unequal spacings between the phases, variations in conductor heights above ground, and skin effect which can cause unequal current division between homogeneous conductors.

Figure 5.3 shows the test case for 1c. Phases B and C are not energized but have a source impedance and a load as specified. This loading was done to reduce the coupling from the energized phase (A). The calculations accurately predict the measurements.

Figure 5.4 shows the test case for 1d where the loads are the same as in test 1c but all three phases are energized. The calculated voltage and current does not predict the experimental voltage or current very well, but some general trends can be seen.

## 5.3. Test Cases with One Phase Extended

In the four configurations of test 2 (Figures 5.5-8), the first segment of line has a three conductor length of $0.5\lambda$ and the second segment is composed of phase A which is extended by $0.16\lambda$.

Figure 5.5a shows the schematic diagram for test 2a with phases B and C floating and the extended segment of phase A grounded at the end. There is good correlation between the measured and calculated results.

Figure 5.6 shows the test case for 2b where the extended segment of A is terminated in an open-circuit. The measured voltage plot in Figure 5.6b shows that the electrical half-wavelength is approximately 2.52 miles instead of 3.54 miles. This corresponds to a velocity factor of 0.68c instead 0.95c. After about 2 miles the calculated plots match the measured data well. A similar profile occurs in each test case where the extended phase is terminated in an open-circuit (see Figures 5.8 and 5.10). Figure 5.7 shows the test case for 2c where all phases are energized and the extended segment is grounded at the load. Again, there is good correlation between the measured and calculated results.

## 5.4. Test Cases with Three Different Line Lengths

In the six configurations of test 3 (Figures 5.9-14), each of the three phases have different lengths. See Figure 5.9a for the schematic diagram showing the three lengths of phases A, B, and C. Figure 5.9 shows the test case for 3a where the extended phase A is grounded and the source is connected only to phase A. There is a fair correlation between the measured and calculated results.

Figure 5.10 shows the test case for 3b where the configuration is the same as that in Figure 5.9 except that phase A has an open circuit load. As

with the test cases in Figures 5.6 and 5.8 a similar voltage profile occurs. The electrical half-wavelength in the experimental case is smaller than classical theory predicts. Again, after about 2 miles the plots match up well.

For the test case in Figure 5.11, phase A is terminated with a load of 410 Ω and the rest of the network is the same as the previous configuration in Figure 5.10. The 410 Ω load on phase A was used as an approximation of the actual single phase characteristic impedance [6]. The experiment and calculation shows that the 410 Ω load is a relatively good termination to cancel the standing wave pattern.

Figure 5.12 shows the test case for test 3d where all phases are energized and phase A is grounded at the load. Since phase C is only a quarter-wavelength, the impedance looking into phase C was very low, causing disproportionate source current to be drawn. As a result, the voltage increases rapidly. The calculations predict this rapid increase well.

Figure 5.13 shows the test case for test 3e where all phases are energized and phase A is terminated in an open circuit. As in Figure 5.12, phase C dominates the other 2 phases with the large voltage and current.

Figure 5.14 shows the last test case where phase A is terminated with a load of 410 Ω. The voltage and current for phase C was omitted since it was similar to that in Figures 5.12 and 5.13 and to emphasize the voltage and current curves for phases A and B. Basically, the calculations show a

higher voltage and current than the measurements but the shapes of the curves match up well.

## 5.5. Conclusions

It is very hard to accurately model the configuration of the distribution lines since several physical parameters are constantly changing. The heights of the lines above the ground and the geometry of the conductors (vertical, horizontal and delta) are variable over the rolling terrain of the test facility. In general, the physical variations cause the calculations that were run from "3-2-1" to predict the location of the nodes and antinodes but kept the magnitudes from being accurately predicted. Another important is that the neutral wire was present in every test case. See the Conclusions in Chapter 7 for more explanation of the results and conclusions found.

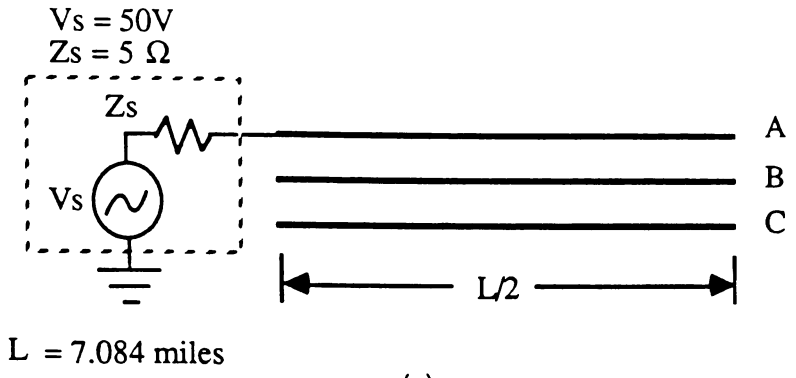


L = 7.084 miles

(a)

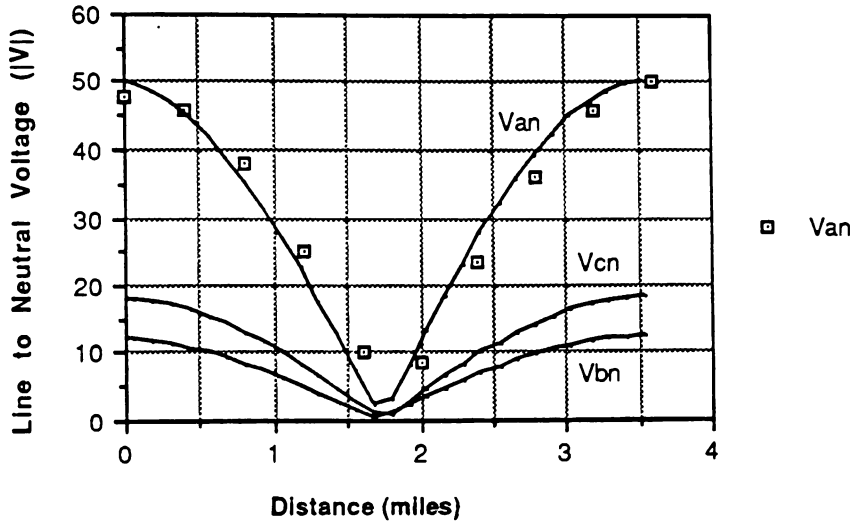


(b)

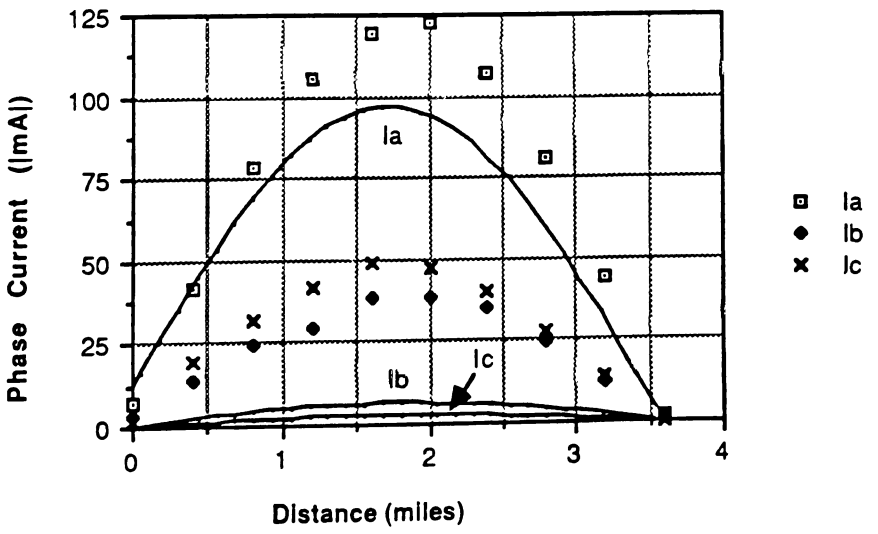


(c)

Figure 5.1 (a) Schematic diagram, (b) voltage plot, (c) current plot for test 1a

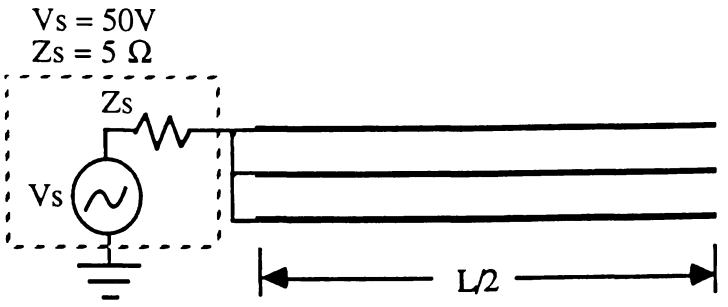


L = 7.084 miles

(a)

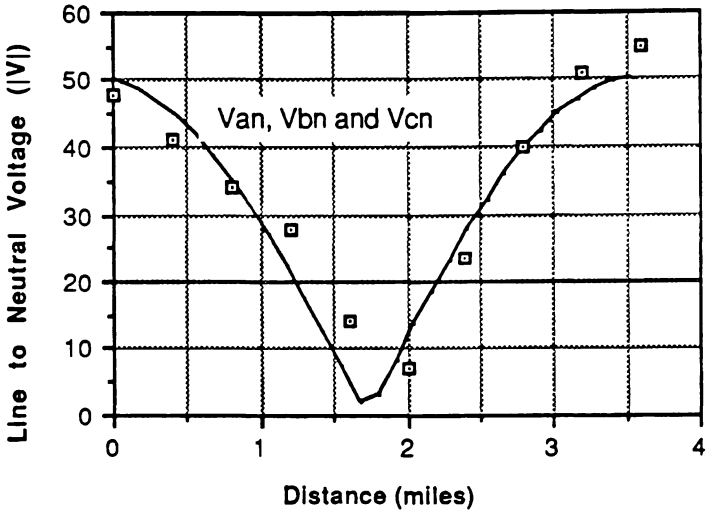


(b)

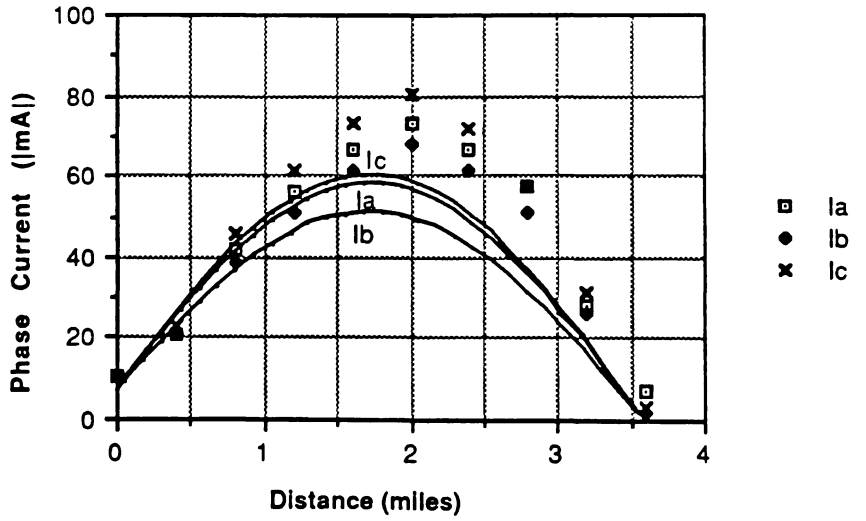


(c)

Figure 5.2 (a) Schematic diagram, (b) voltage plot, (c) current plot for test 1b

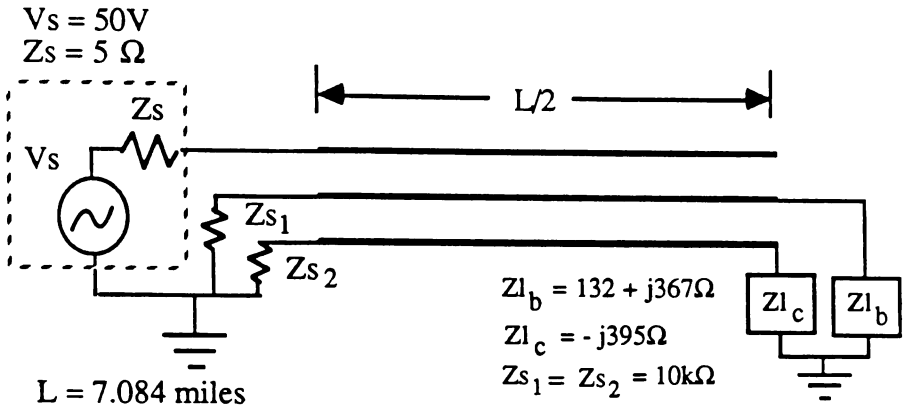


(a)

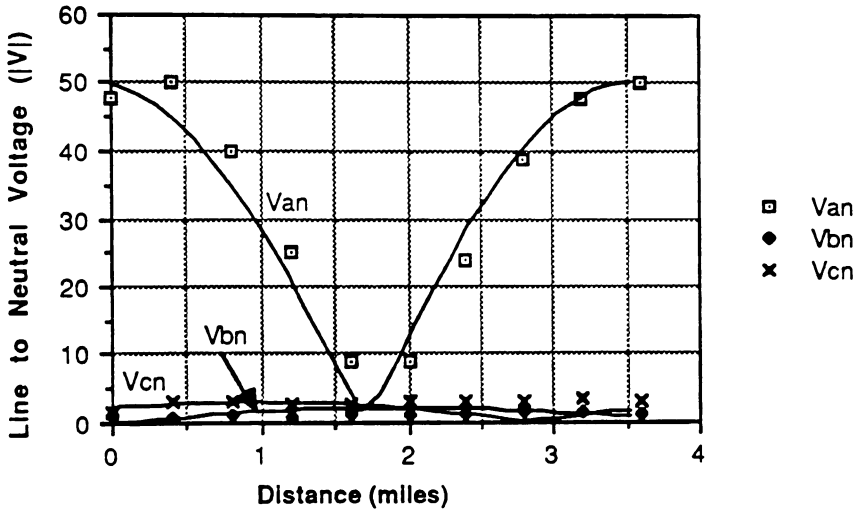


(b)

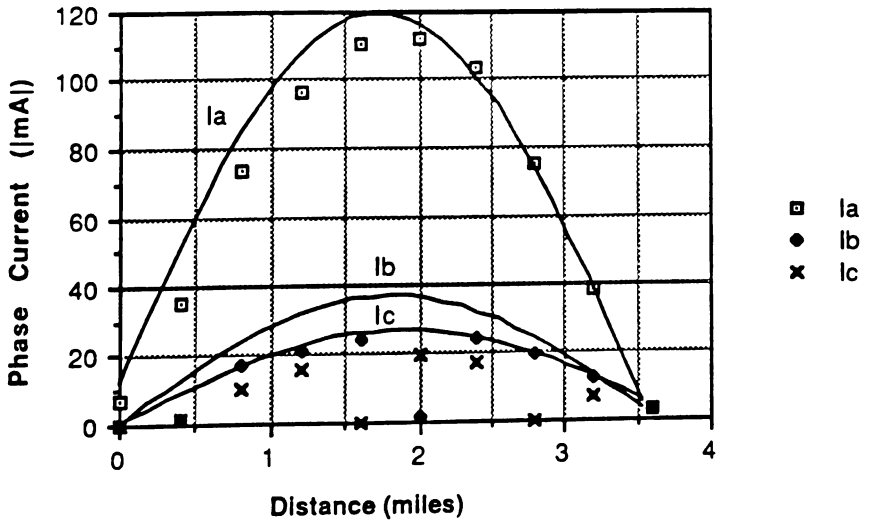


(c)

Figure 5.3 (a) Schematic diagram, (b) voltage plot, (c) current plot for test 1c

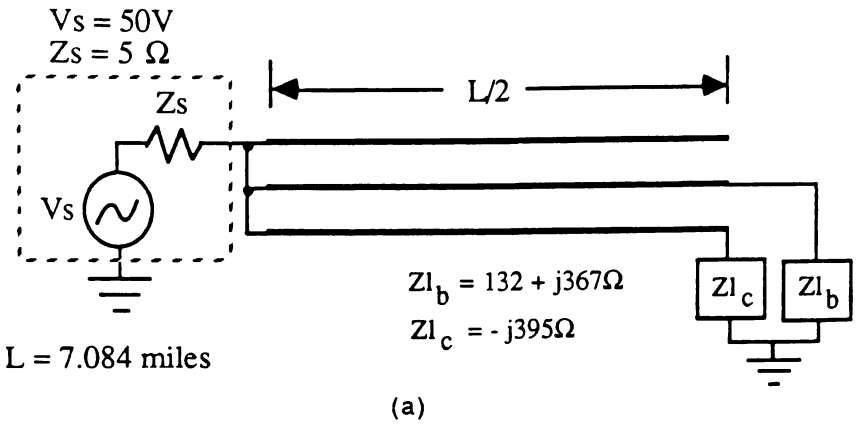


(a)

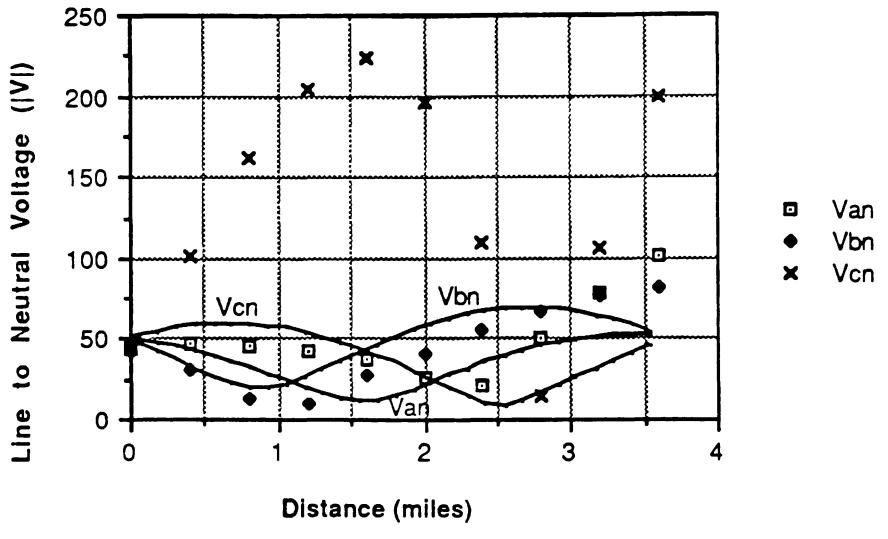


(b)

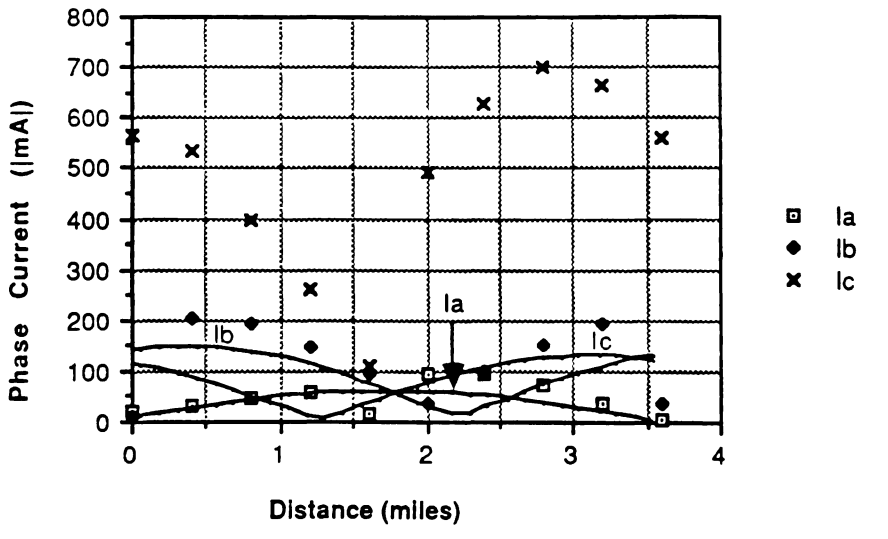


(c)

Figure 5.4 (a) Schematic diagram, (b) voltage plot, (c) current plot for test 1d

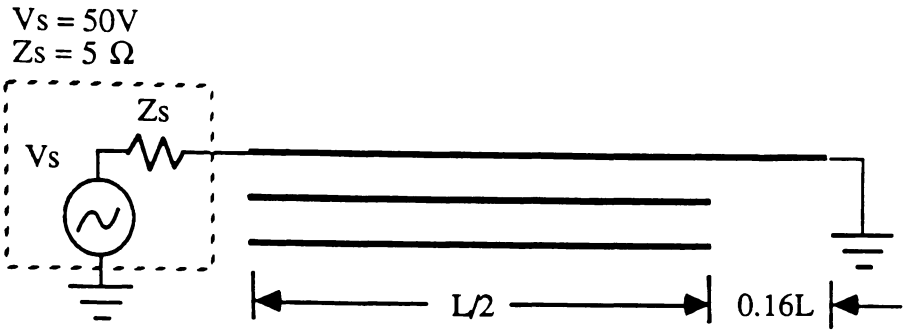


(a)

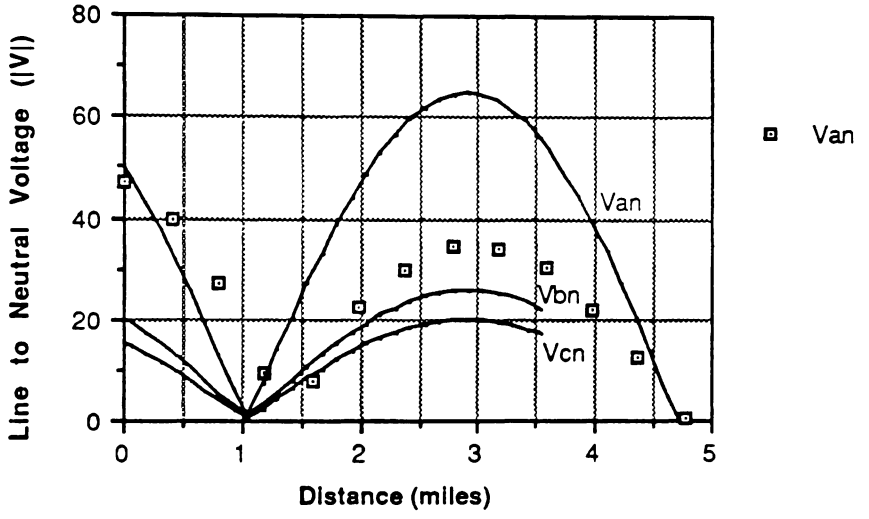


(b)

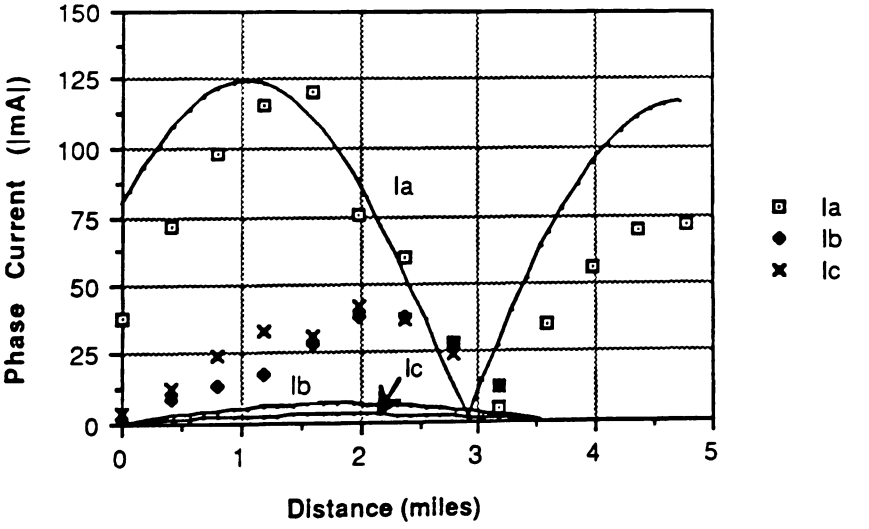


(c)

Figure 5.5 (a) Schematic diagram, (b) voltage plot, (c) current plot for test 2a

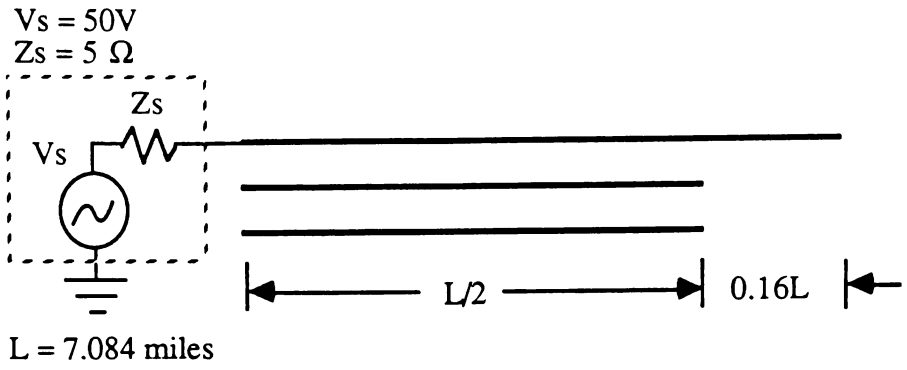


(a)

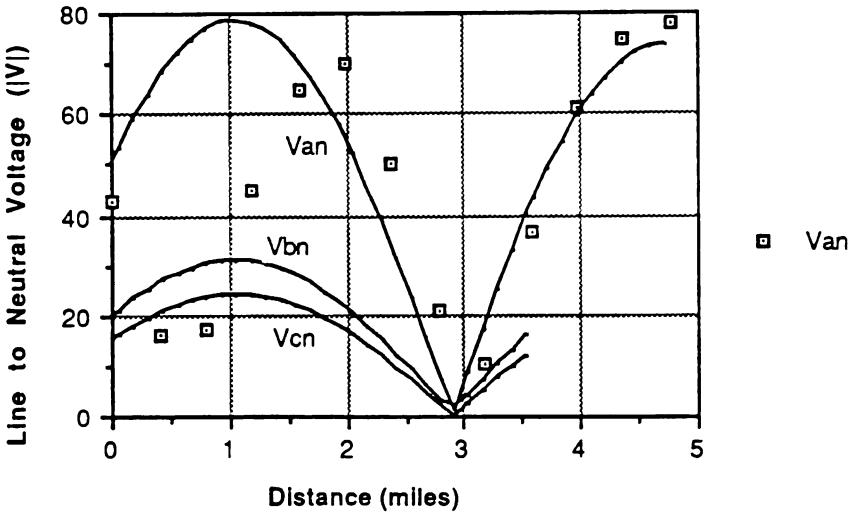


(b)

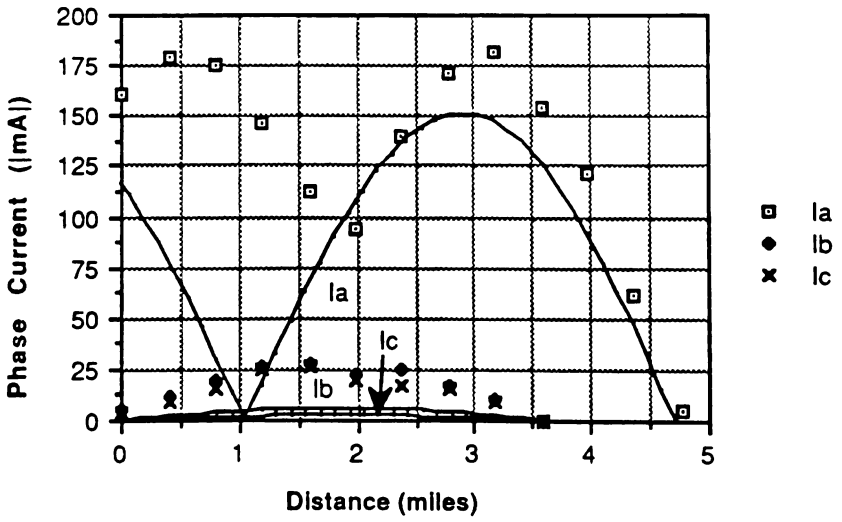


(c)

Figure 5.6 (a) Schematic diagram, (b) voltage plot, (c) current plot for test 2b

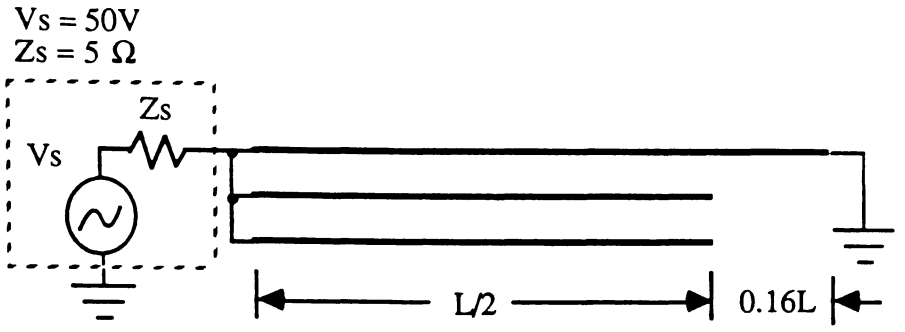


(a)

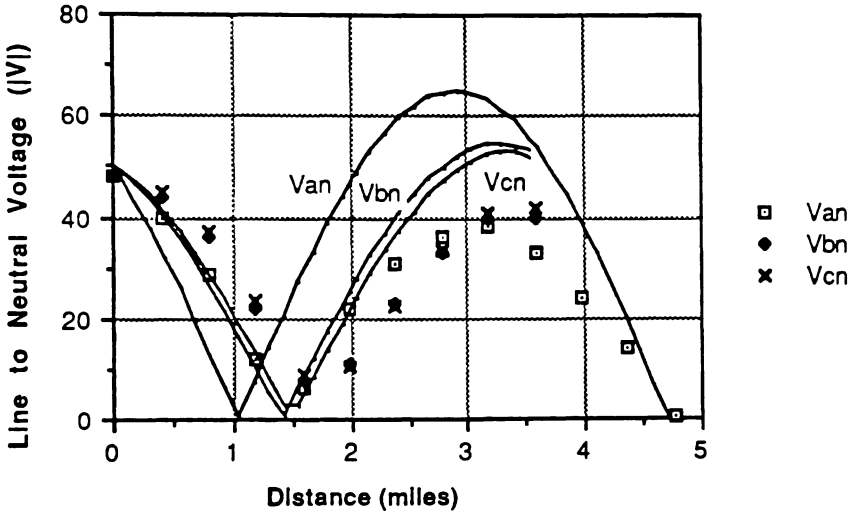


(b)

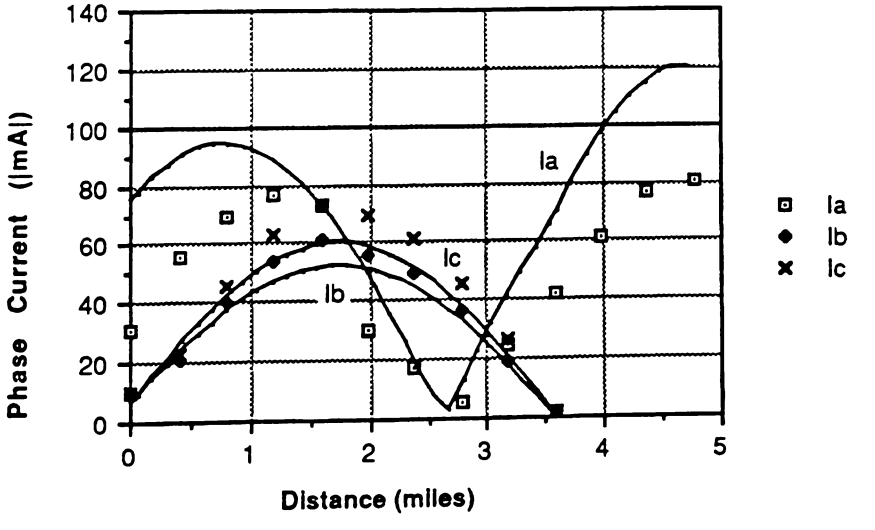


(c)

Figure 5.7 (a) Schematic diagram, (b) voltage plot, (c) current plot for test 2c

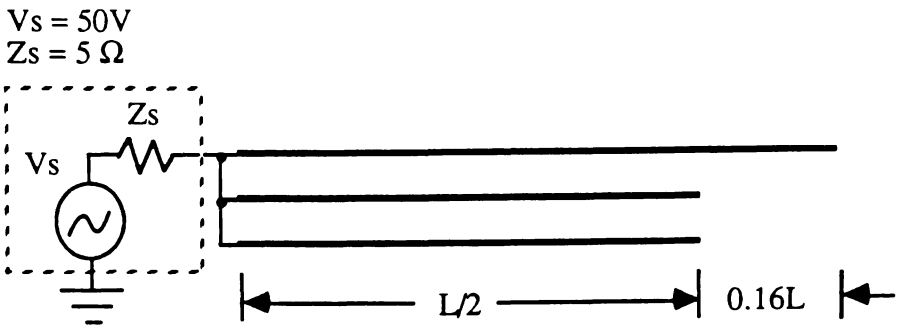


(a)

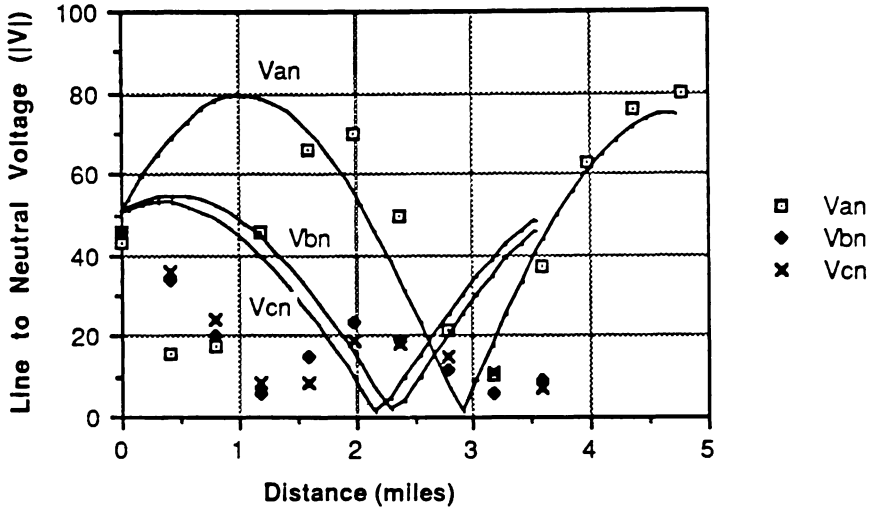


(b)

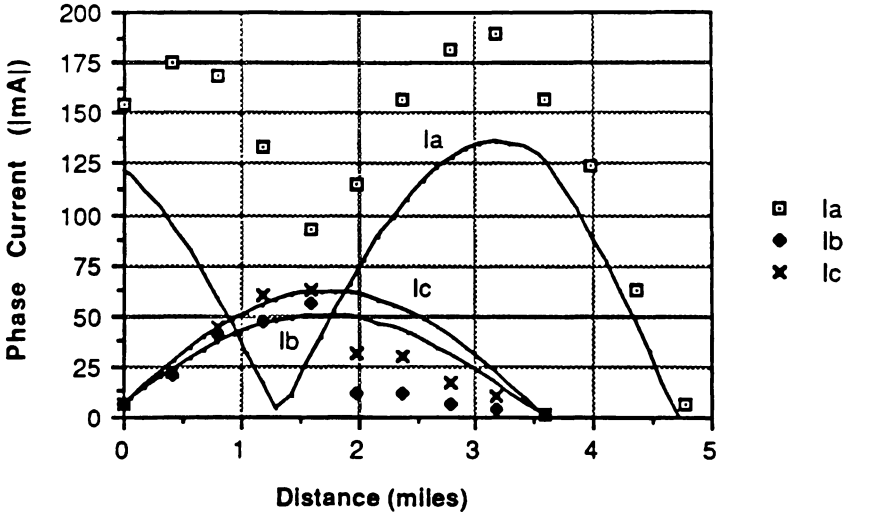


(c)

Figure 5.8 (a) Schematic diagram, (b) voltage plot, (c) current plot for test 2d

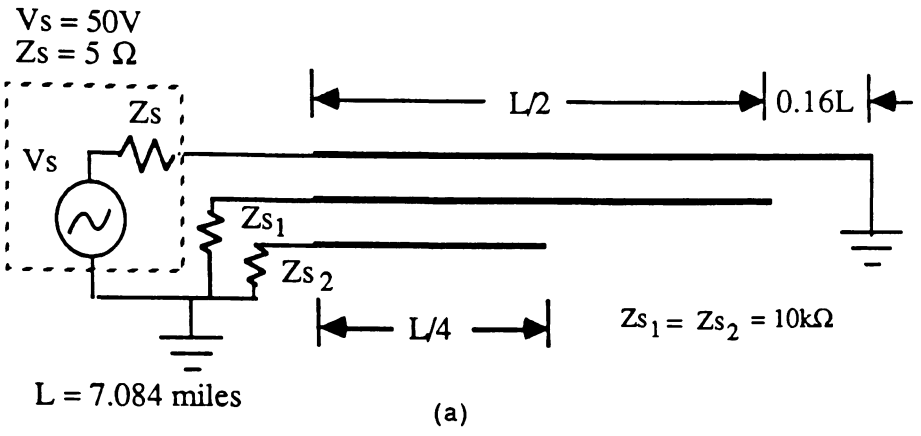


(a)

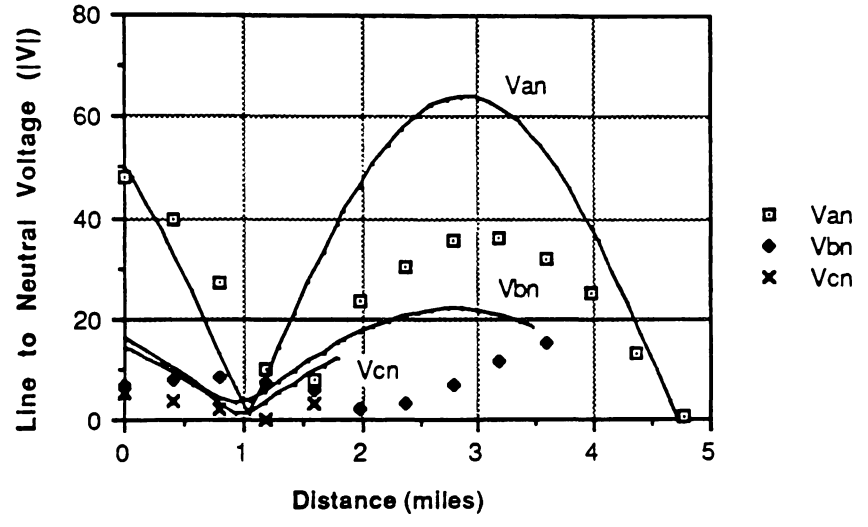


(b)

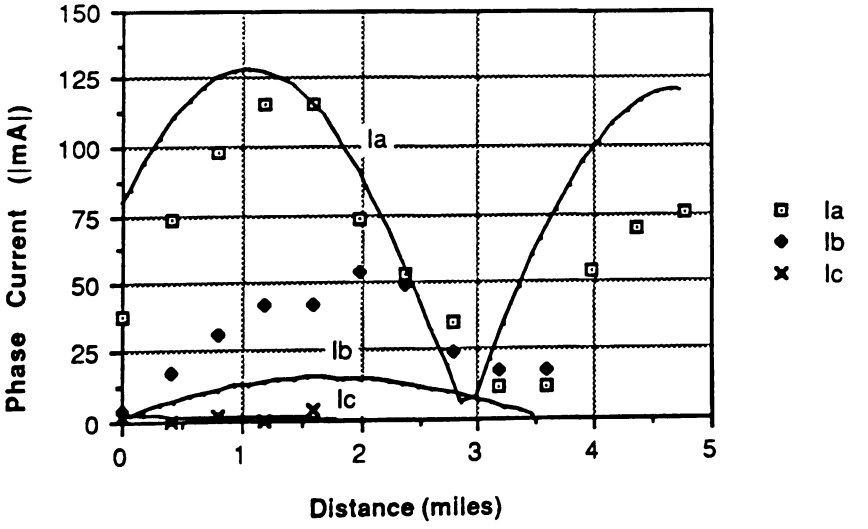


(c)

Figure 5.9 (a) Schematic diagram, (b) voltage plot, (c) current plot for test 3a

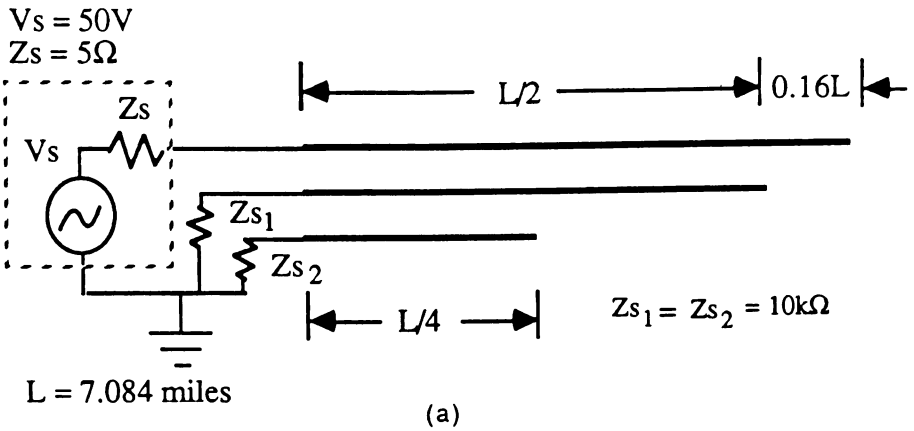


(a)

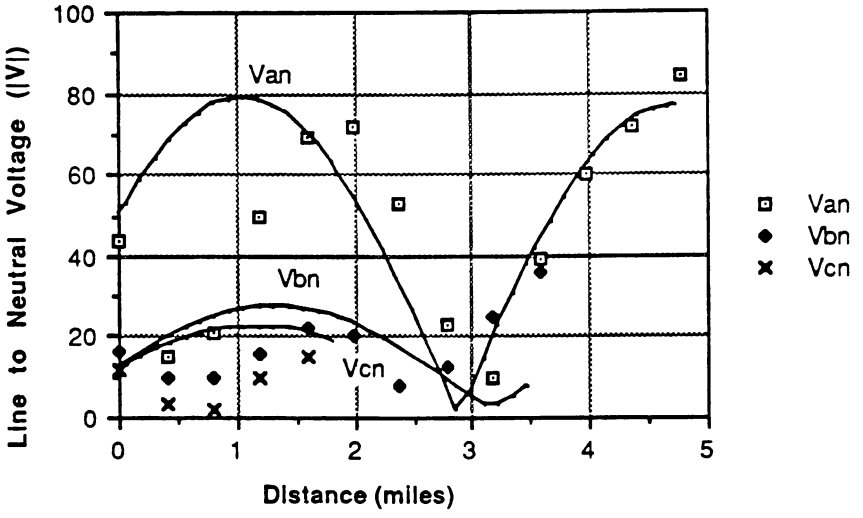


(b)

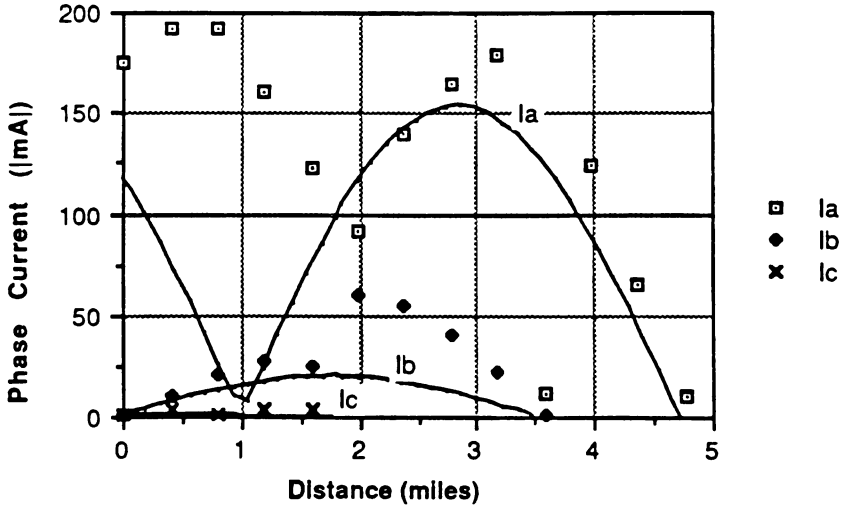


(c)

Figure 5.10 (a) Schematic diagram, (b) voltage plot, (c) current plot for test 3b

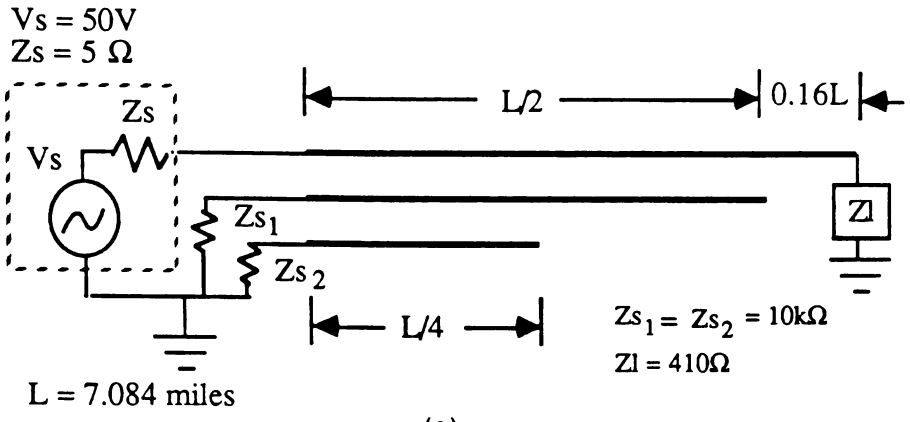


(a)

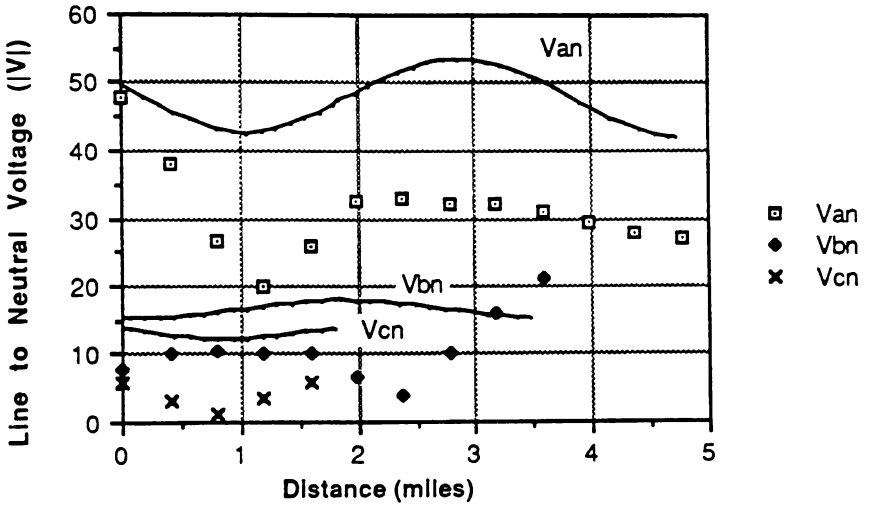


(b)

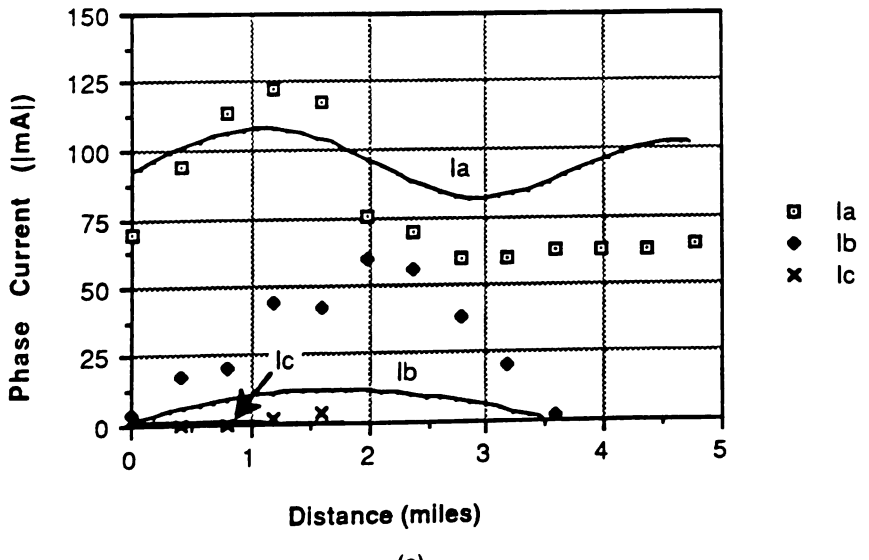


(c)

Figure 5.11 (a) Schematic diagram, (b) voltage plot, (c) current plot for test 3c

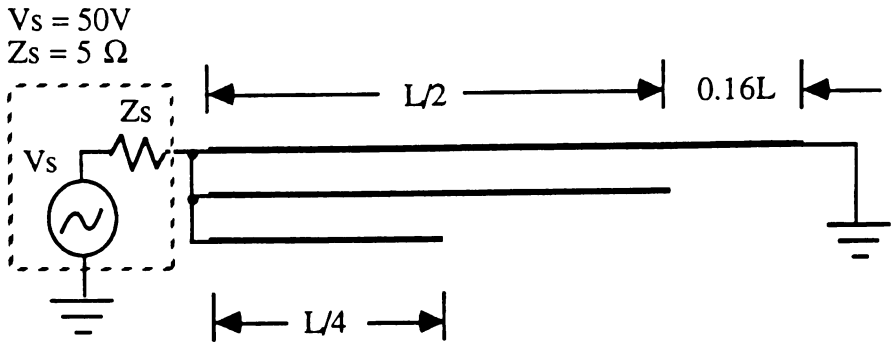


L = 7.084 miles

(a)

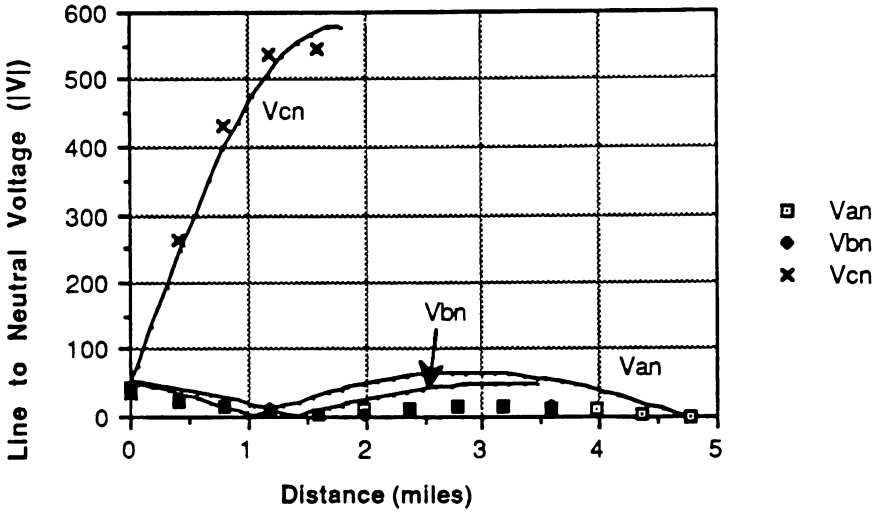


(b)

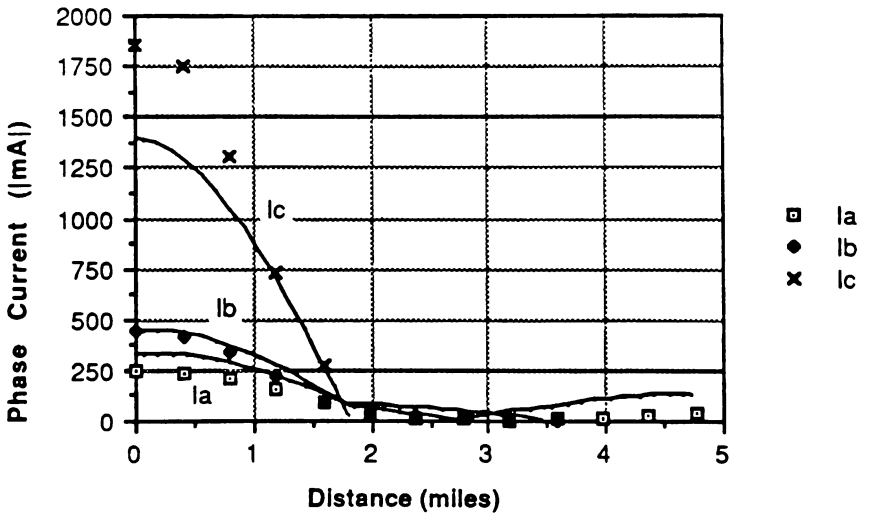


(c)

Figure 5.12 (a) Schematic diagram, (b) voltage plot, (c) current plot for test 3d

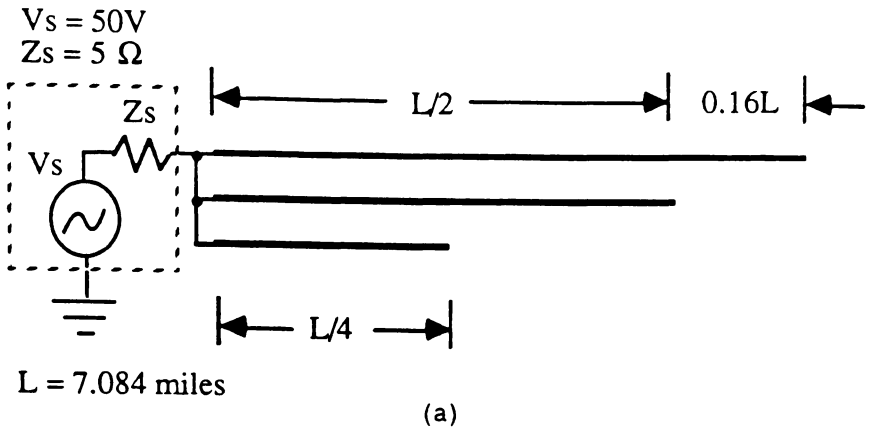


(a)

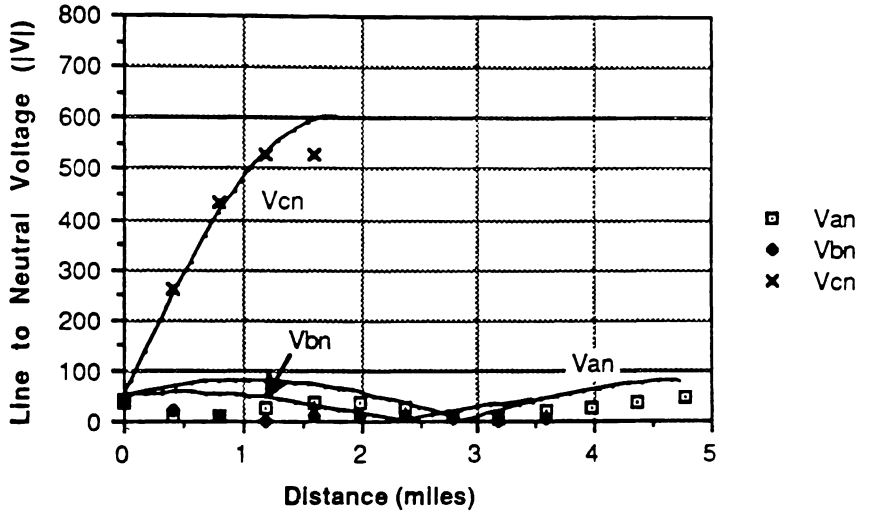


(b)

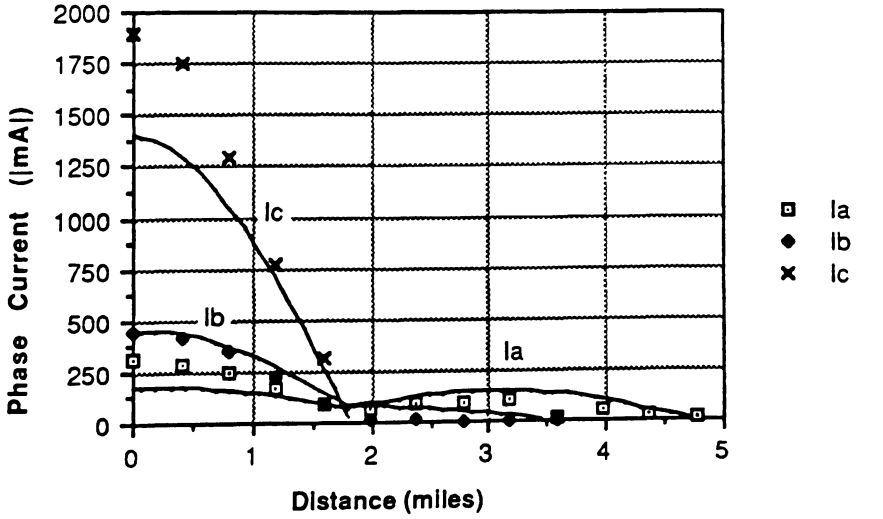


(c)

Figure 5.13 (a) Schematic diagram, (b) voltage plot, (c) current plot for test 3e

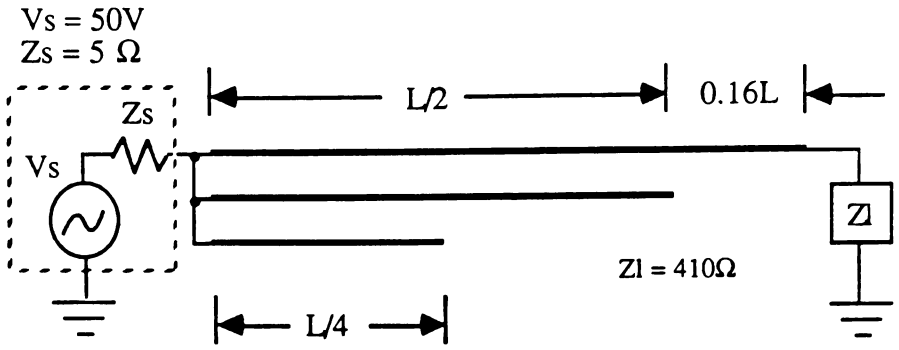


L = 7.084 miles

(a)

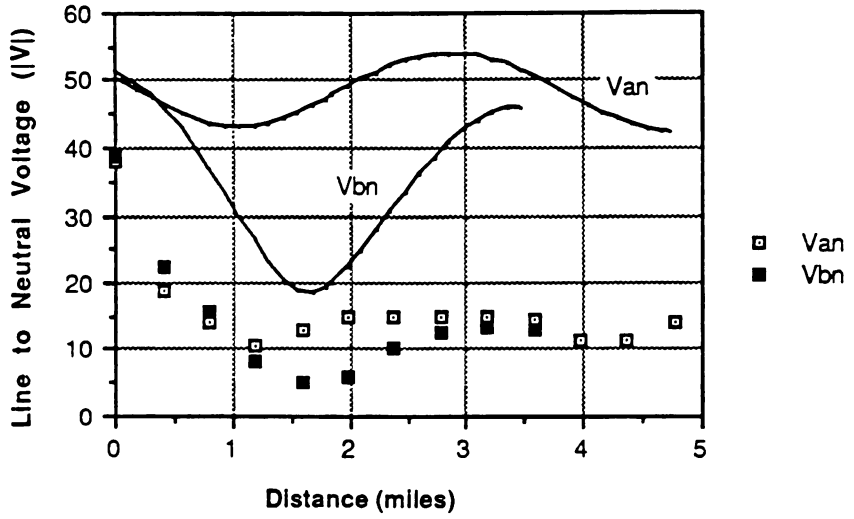


(b)

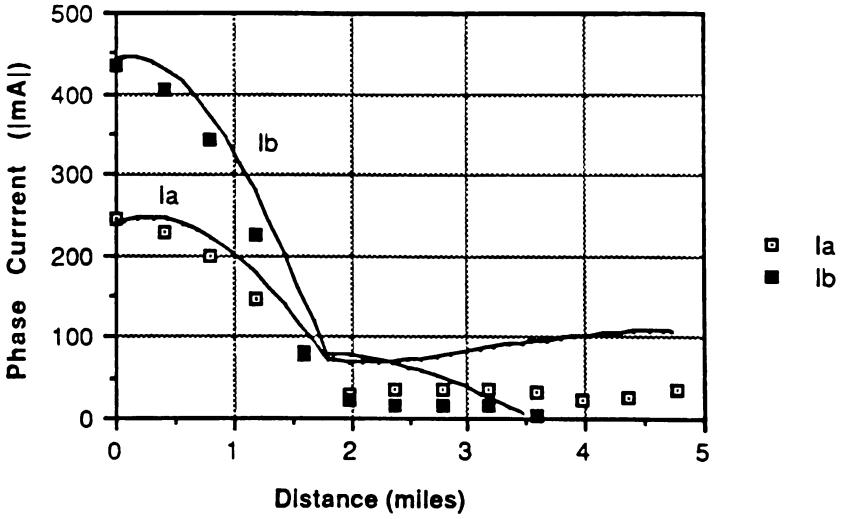


(c)

Figure 5.14 (a) Schematic diagram, (b) voltage plot, (c) current plot for test 3f

# Chapter 6

## Test Cases with the Calculated Characteristic Impedance as the Load

### 6.1. Introduction

It is well known that when a load equal to the characteristic impedance is placed at the end of a single-phase lossless distribution line, there is no reflected wave [18]. The voltage and current are constant along the line. In reality, all distribution lines have some loss, therefore the voltage and current will vary slightly along the line. This chapter presents several calculated test cases where the calculated characteristic impedance is placed at various locations along the line and the results are discussed.

### 6.2. Calculations

Figure 6.2 shows the first test case where the configuration in test 1b (Figure 5.2) is modified to terminate it with the calculated characteristic impedance instead of an open-circuit. The calculated voltage plot in Figure 6.2b shows all 3 phases matched, therefore there is no standing wave. Also, since the voltage decreases very slightly, the distribution line is considered lossless. Figure 6.2c shows the calculated current plot with a similar attenuation. As mentioned before, the currents are not equal along the line because of skin effect and the unequal spacings between the conductors.

In Figure 6.3, the characteristic impedance is placed at the source to ground and at the end of the line. (Note: this configuration can be analyzed

by slight modifications in the source code in the appendices. "3-2-1" was later modified to handle loads at the source to ground.) As expected, the voltage and current profiles are the same as in Figure 6.2. To verify this refer to Figure 1; $Y_{sg} = Y_{in}(0) = Y_o$ and therefore $Y'_{in}(0) = 2Y_{in}(0)$. $V(0)$, as before, is approximately $V_s$ since $Z_s$ is small. Now $I(0) = V(0)$ $Y'_{in}(0)$ which is approximately $2V_sY_{in}(0)$. Finally, $I'(0) = I(0)$ $\left(Y_{in}(0)\ Y'_{in}(0)^{-1}\right)$ which is approximately $V_sY_{in}(0)$ which is the same initial current as in Figure 6.2.

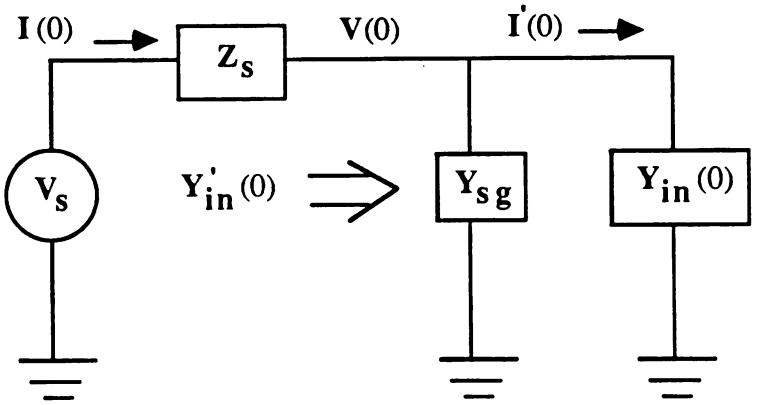


Figure 6.1. Schematic diagram showing the variation of the impedance seen at the source with a source to ground load (a modification of Figure 2.2)

In Figure 6.4, the characteristic impedance is placed at a half-wavelength and the line is extended a half-wavelength farther. Figure 6.4b shows that the voltage is relatively flat for the first half-wavelength and then a half standing wave for second half-wavelength. The first segment is not exactly flat since the source "sees" not only the characteristic impedance but the open-circuit at the end "rolled" back and combined with the characteristic impedance at the first node. Similar results occur for the

current in Figure 6.4c but notice the large magnitude of current in the second half-wavelength.

In Figure 6.5, the characteristic impedance is placed at a quarter-wavelength and the line is extended three quarters of a wavelength farther. Notice that when the characteristic impedance is placed at this point it has little or no effect on cancelling the standing wave pattern (see the reasoning mentioned above).

In Figure 6.6, test 1d (Figure 5.4) is modified to include the characteristic impedance at one wavelength. A similar wave pattern occurs as in Figure 5.4b and c for the first half-wavelength and flattens out for the second half-wavelength. Note that even though phase A only has the characteristic impedance at a wavelength, voltage is induced from phases B and C for the first half-wavelength and a standing wave results.

In Figure 6.7, the characteristic impedance is placed at a half-wavelength and a wavelength. A standing wave results for the first half-wavelength and then flattens out for the second half-wavelength. In this case, the source "sees" *half* of the characteristic impedance and the first node "sees" the *whole* characteristic impedance at the end.

## 6.3. Conclusions

The calculations in Figures 6.2 and 6.3 agree with theory [18]. The characteristic impedance is placed at the end of a line, the line is matched, therefore a standing wave pattern does not occur. Figures 6.4-7 present

some interesting cases where the characteristic impedance and other loads are placed at various points along the line. These cases can provide new insight into the characteristics of distribution lines. In Figures 6.6-7, a standing wave results for the first half-wavelength and the line is matched for the second half-wavelength. The reason for this is that in each case the impedance seen looking into the second half-wavelength is the just the characteristic impedance at the end of the line. In essence, if the characteristic impedance is placed at the end of the line then the line will be matched until the next load up the line is reached, or a branch is encountered (see Figure 6.8).

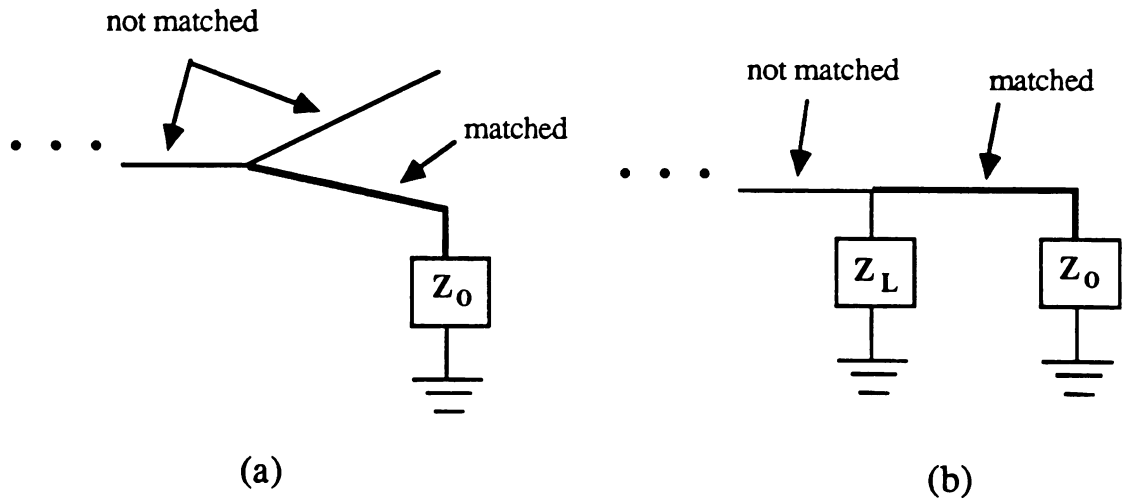


Figure 6.8 Portion of a distribution line network terminated by the characteristic impedance, (a) line is matched until a previous section branches, (b) line is matched until previous load is reached

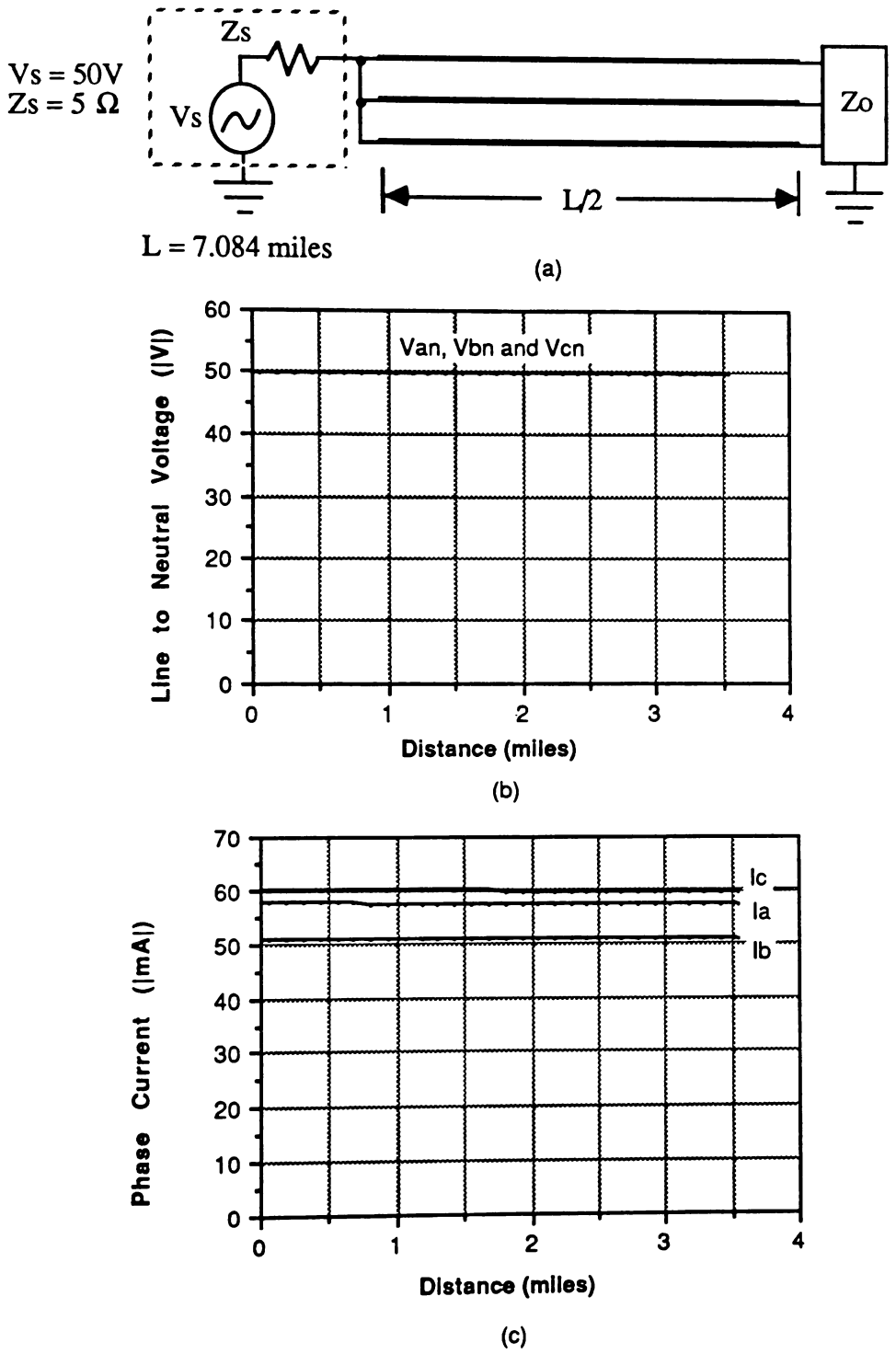


Figure 6.2 (a) Schematic diagram, (b) calculated voltage plot,
(c) calculated current plot for characteristic impedance at load

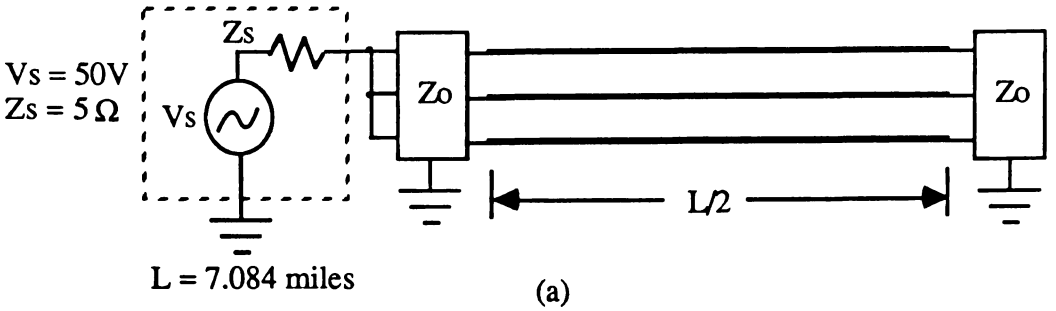


(a)

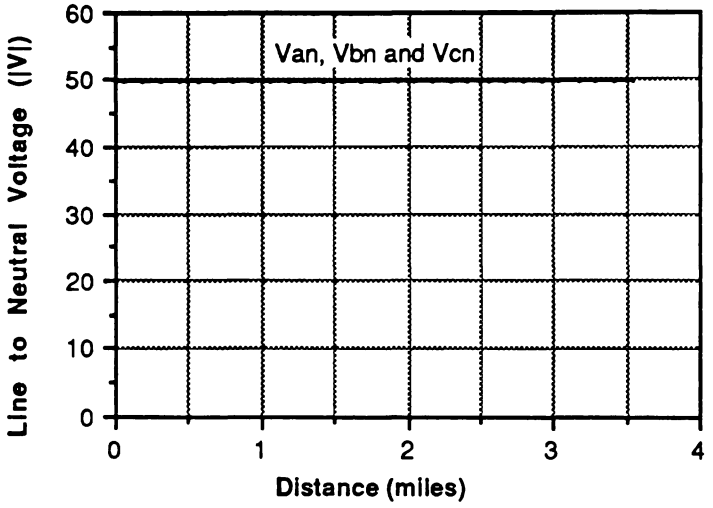


(b)

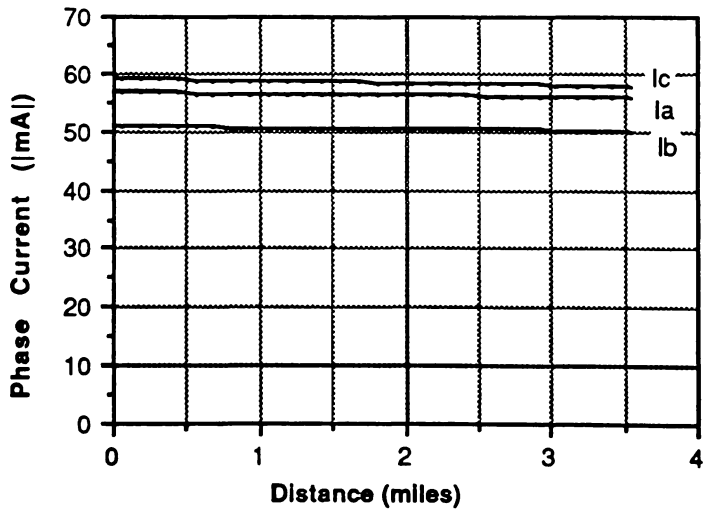


(c)

Figure 6.3 (a) Schematic diagram, (b) calculated voltage plot, (c) calculated current plot for characteristic impedance at source and load

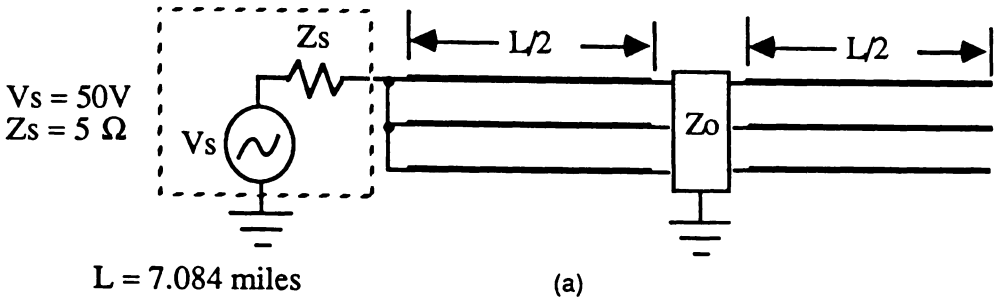


L = 7.084 miles

(a)

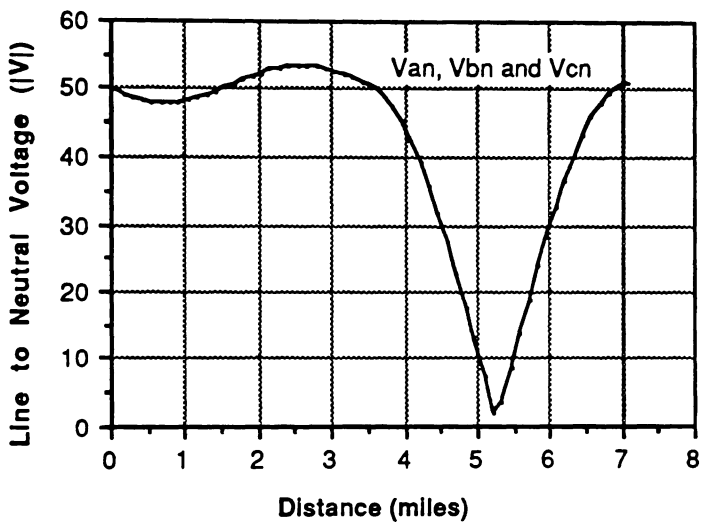


(b)

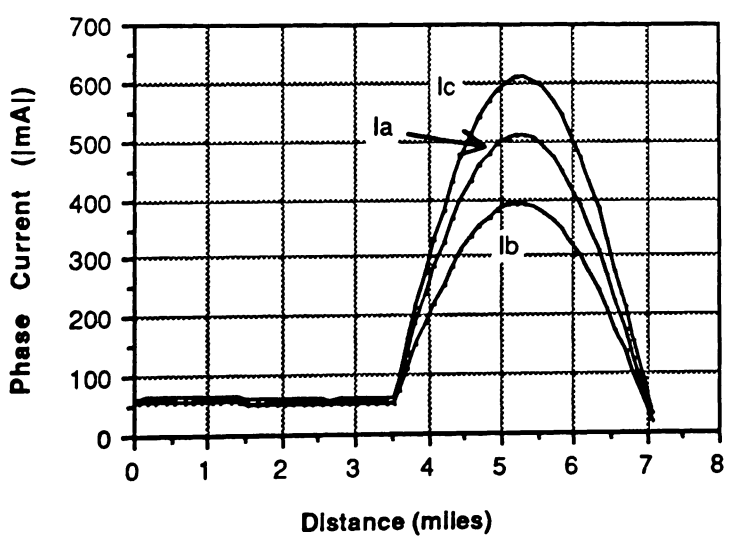


(c)

Figure 6.4 (a) Schematic diagram, (b) calculated voltage plot, (c) calculated current plot for characteristic impedance at L/2 and open at the end

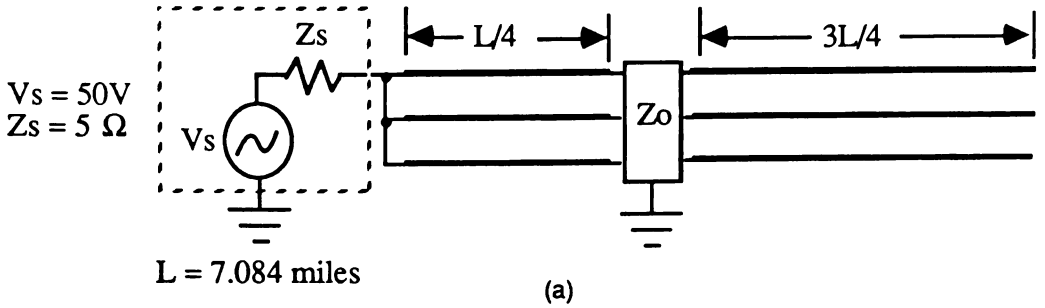


(a)

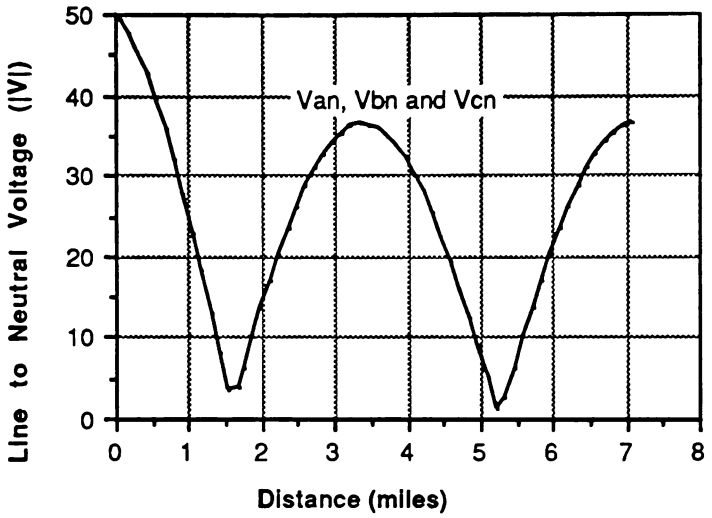


(b)

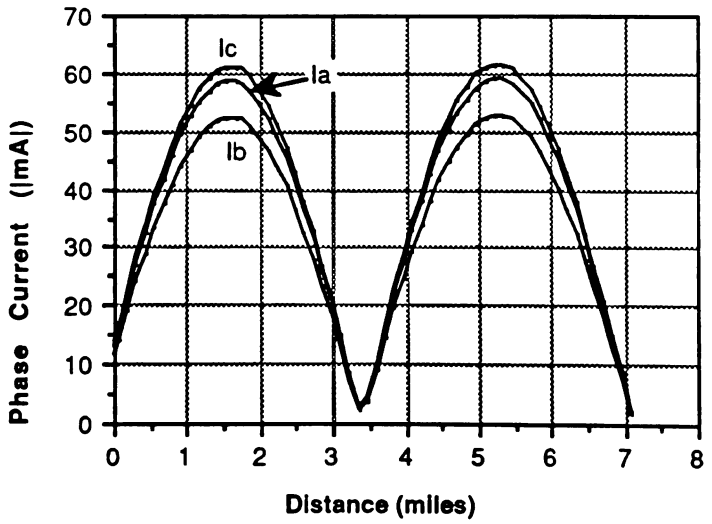


(c)

Figure 6.5 (a) Schematic diagram, (b) calculated voltage plot, (c) calculated current plot with characteristic impedance at L/4

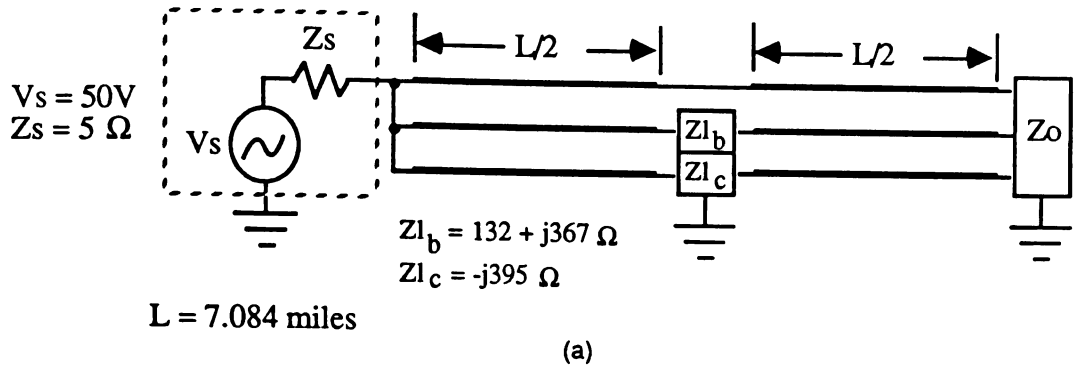


(a)

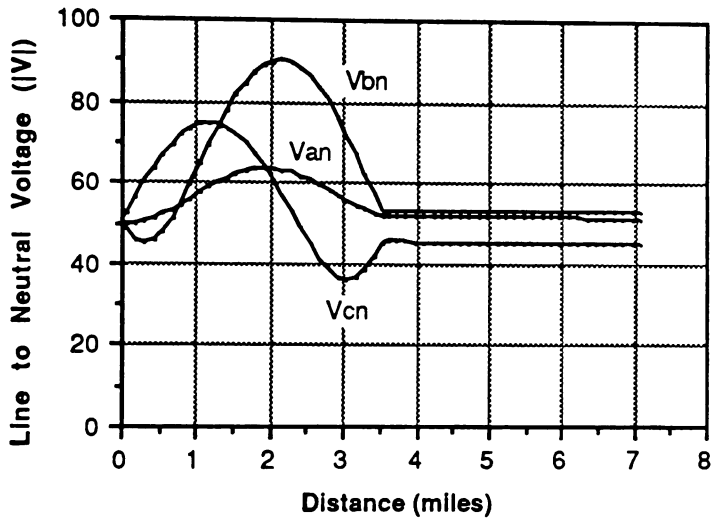


(b)

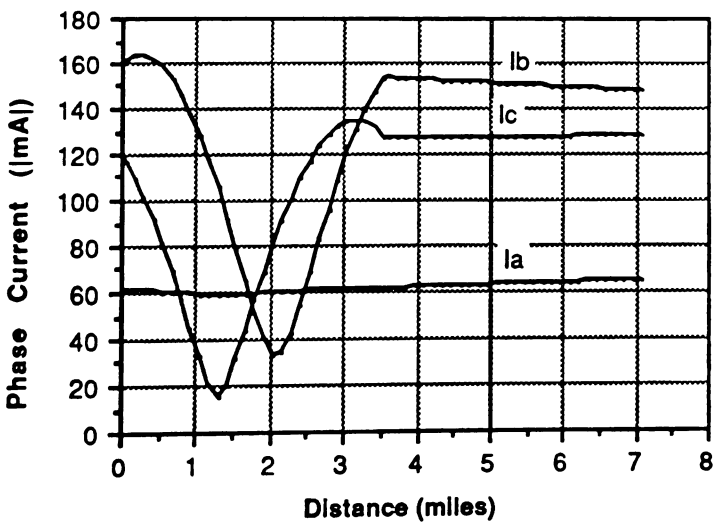


(c)

Figure 6.6 (a) Schematic diagram, (b) calculated voltage plot, (c) calculated current plot for test 1d modified

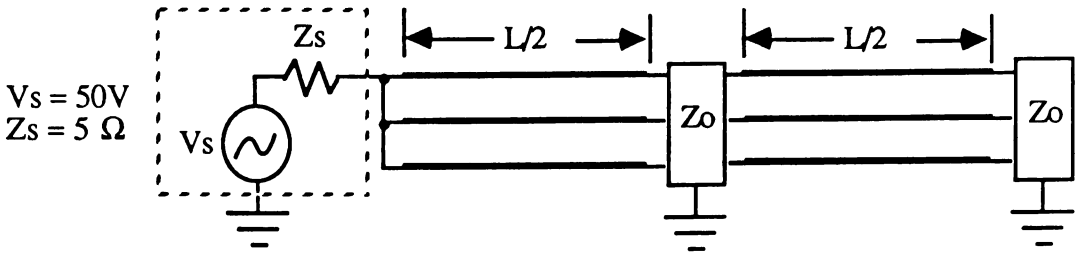


L = 7.084 miles

(a)

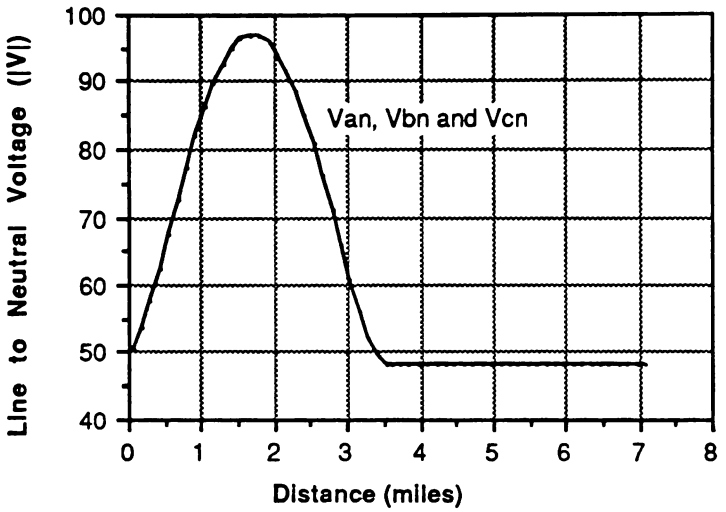


(b)

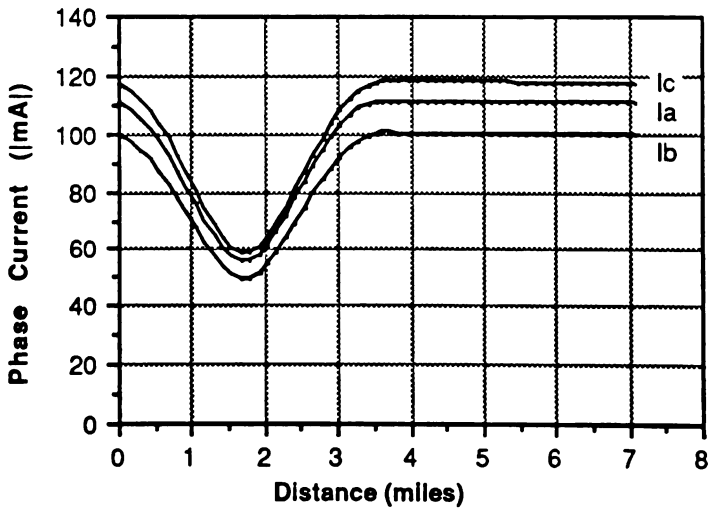


(c)

Figure 6.7 (a) Schematic diagram, (b) calculated voltage plot, (c) calculated current plot with characteristic admittance at L/2 and L

# Chapter 7

# Conclusions

The computer program "3-2-1" was implemented to predict multiconductor signal propagation in distribution line carrier (DLC) networks. The program can model distribution line networks that have three phases at the source and go from three phases to two phases to a single phase with loads distributed anywhere along the line. The user can specify the conductor geometry (i.e. spacing between the phases and height above the ground) and the ACSR conductor properties (i.e. number of inner and outer strands and the radius of the inner and outer strands). The calculated characteristic impedance or any scalar factor of it can be used as a load.

Several calculations were run and the results were compared with experimental measurements (Chapter 5) made by Suh [6]. More calculations were run to examine the effects of terminating the distribution line with the characteristic impedance matrix, $\mathbf{Z_o}$ (Chapter 6). The following general conclusions can be made from the research and calculations done:

(1) Based on the multiconductor line equations (Chapter 2), the computer calculations predict the experimental results well. In almost every case the trends between the theoretical and experimental results match up. However, in most cases the

magnitude of the calculated voltage and current were not as large as the experimental results.

(2) An accurate method to calculate the per-unit length impedance (**Z**) and admittance (**Y**) matrices (Chapter 3) was implemented. The skin effect resistance, $R_{se}$, is calculated by modeling the stranded conductor as a hollow conductor. It was found that an accurate calculation of $R_{se}$ is important since it directly affects the characteristic impedance matrix, $\mathbf{Z_o}$.

(3) It is verified in Chapter 6 that terminating a distribution line with the characteristic impedance eliminates the standing wave pattern in the voltage and current waveforms. It was also found that when the characteristic impedance is placed at the end of the line then the line will be matched until the next load up the line is reached or a branch is encountered.

The inaccuracy of some of the predictions is likely to be caused by the many assumptions that were made in using the theoretical model. Among these are:

(1) The conductor geometry varies from the vertical to horizontal to the delta configuration. In each calculation, the vertical configuration was assumed (see Figure 3.2).

(2) It was assumed that all of the primary current returns through the earth's surface. However, Hemminger [4] found that

approximately 30% of the primary current returns through the neutral wire except for a few poles at either end of the line. This value depends on several factors such as the temperature, humidity, soil moisture content and the type of soil. Also, the test facility terrain is over rolling hills causing the height of the conductors to vary.

(3) The earth's conductivity was modeled as a known constant. In reality it varies from place to place.

(4) In the cases with unequal line lengths (Figures 5.9 - 14), the calculations were based on the absence of the conductor on the far end on phases B and C. In reality, the line had three phase conductors plus the neutral wire throughout. Phases B and C were simply opened to simulate the line going from three to two to one phase. Four conductors were always present on the poles for all measurements even though some had been opened.

Work is being done to develop a better model for the distribution line network. Improvements in the model include:

(1) Modeling the earth return including earth resistivity. In the present model a perfectly conducting ground plane was assumed.

(2) The neutral wire must be incorporated into the model. In this case a five conductor system (the three phase conductors, the neutral wire and the ground plane) must be solved instead of a

four conductor system. This is important since (1) a small percent of the return current flows through the neutral wire, (2) voltage and current is induced in the neutral wire, and (3) the neutral wire changes the per-unit parameters and is generally grounded at every pole.

In conclusion, complex distribution line networks can be mathematically modeled accurately. If the physical distribution line network can be characterized accurately taking into account the factors mentioned above to calculate the **Z** and **Y** per-unit length matrices, then results can be obtained that will match very well with experimental measurements. Further research is being done to model tree-structured systems which handles branching, and network synthesis where loads can be designed and placed at existing nodes to cancel standing wave patterns.

# REFERENCES


1. "RF Model of the Distribution System as a Communication Channel," vols., 1, 2, 3, 4, 5 and 6, December 1978, Contract No. EC-77C-01-2100, Report by General Electric Company, Corporate Research and Development, Schenectady, NY; Prepared for U.S. Department of Energy, Division of Electrical Energy System, Washington, D.C.

2. "RF Model of the Distribution System as a Communication Channel," Phase II-4 volumes, Contract No. 955647, July 28, 1982, General Electric Company, Corporate Research and Development, Schenectady, NY 12345

3. "The Distribution Automation 23 kV Test Facility, An Introduction," Carolina Power and Light Company Introductory Report, Raleigh, NC May 16, 1984.

4. Hemminger, Rodney C., "The Effect of Distribution Transformers on Carrier Signal Propagation for a Power Distribution Line at Power Line Carrier Frequencies," Master's Thesis, North Carolina State University, 1985.

5. Borowski, Daniel, "Simulated Signal and Noise Profiles in Distribution Line Carrier Networks," Master of Science Thesis, North Carolina State University, 1986.

6. Suh, John D., "Multiconductor Signal Propagation in Distribution Line Carrier Networks," Master's Thesis, North Carolina State University, 1988.

7. Riddle, M., Ardalan, S. and Suh, J., "Derivation of Voltage and Current Transfer Functions for Multiconductor Transmission Lines," International Symposium of Circuits and Systems, Portland, OR. 1989

8. Riddle, Michael L., "Modeling Multiple Conductor Transmission Lines," Master's Thesis, North Carolina State University, 1988.

9. Paul, C.R. and Feather, A.E., "Computation of the Transmission Line Inductance and Capacitance Matrices from the Generalized Capacitance Matrix," IEEE Transactions on Electromagnetic Compatibility, vol. EMC-18, Nov. 1976.

10. Woodruff, L.F., Principles of Electric Power Transmission, New York: John Wiley and Sons, Inc., second edition, 1956.

11. "Aluminum Electrical Conductor Handbook," The Aluminum Association, first edition, September, 1971

12. Reference Data for Radio Engineers, Howard W. Sams & Co., Inc., 1975 Indianapolis, Indiana 46268

13. "Electrical Characteristics of A.C.S.R.," Aluminum Association of America, Revised November, 1934.

14. Dwight, H. B. "Skin Effect in Tubular and Flat Conductors," AIEE Transactions, 1918, pg. 1379.

15. Norris, F. W. and Bingham, L. A., Electrical Characteristics of Power and Telephone Transmission Lines, Scranton, P.A.: International Textbook Co., 1936.

16. Kochan, Stephen G., Programming in C, first edition, Howard W. Sams & Co., 1983

17. Sobelman, G.E. and Krekelberg, D.E., Advanced C: Techniques & Applications, Que Corp., Indianapolis, Indiana, 1985

18. Kraus, John D., Electromagnetics, third edition, McGraw-Hill Inc., 1984.

19. Anderson, P., Analysis of Faulted Power Systems, The Iowa State University Press, Ames, Iowa, 1973.

20. Stevenson, William D., Elements of Power System Analysis, third edition, McGraw-Hill Inc., 1975.